Exploring Targeted Thorium Conjugate and Small Molecule Combinations: New Effective Treatments for Cancer

Thesis for degree of Philosophiae Doctor

by

Katrine Wickstrøm

Department of Biosciences

The Faculty of Mathematics and Natural Sciences

UNIVERSITY OF OSLO

Series of dissertations submitted to the
Faculty of Mathematics and Natural Sciences, University of Oslo
No. 2105

ISSN 1501-7710

Cover: Hanne Baadsgaard Utigard.
Print production: Reprosentralen, University of Oslo.

Contents

1 Preface

i. Acknowledgements

The presented work was carried out at Bayer AS in Oslo, at Bayer AG in Berlin, at the Norwegian Radium Hospital (DNR) and at the Department of Biosciences (IBV) at the University of Oslo from 2015-2019. The project was supported by Bayer AS and the Norwegian Research council (NFR) (Grant number 246531/030), which I gratefully acknowledge.

First, I would like to express my appreciation to my main supervisor Dr. Alan Cuthbertson for initiating the PhD project, for support and critical review of the work. I have really appreciated all scientific discussions and your encouragement. Further, I wish to express my most sincere gratitude to supervisors Dr. Jenny Karlsson and Dr. Urs Hagemann for the great support throughout the project.

I would like to thank all my colleagues in the TCR team in Oslo for good collaboration and interesting scientific and non-scientific discussions, I feel extremely lucky to be part of a team with so many great people and excellent scientists. I am particularly grateful to Dr. Alexander Kristian and Dr. Christine Ellingsen for training, support and technical assistance during the animal experiments, as well as for their review of the work.

I am grateful to colleagues in Berlin and Wuppertal for good scientific discussions and technical support. I wish to acknowledge the help provided by Dr. Gerhard Siemeister, for welcoming me to his group in Berlin and his assistance in establishing the isobologram assay in Oslo.

I would like to thank my supervisor at the University of Oslo, Dr. Bernd Thiede, for administrative support and for welcoming me to his lab.

I would like to thank my friends, especially the Rorvik dream team, Malin, Jeannette, Marlene and Gro, for their great support throughout the whole PhD. Last but not least, I would like to thank my dear family for their love and encouragement, especially Espen for being so patient and supporting during these years.

Oslo 2019, Katrine Wickstrøm

ii. List of abbreviations

^{227}Ac	Actinium-227
ADC	Antibody drug conjugate
ADCC	Antibody dependent cell mediated cytotoxicity
ADCP	Antibody dependent cellular phagocytosis
APE1	Apurinic/apyrimidinic endonuclease 1
ATM	Ataxia telangiectasia mutated kinase
ATR	Ataxia telangiectasia and Rad3 related
BER	Base excision repair
BRCA1	Breast cancer type 1 susceptibility protein
BRCA2	Breast cancer type 2 susceptibility protein
BW	Body weight
CAR	Chelator to antibody ratio
CDC	Complement dependent cytotoxicity
CDR	Complementarity determining region
Chk1	Checkpoint kinase 1
Chk2	Checkpoint kinase 2
CI	Combination index
CRC	Colorectal cancer
CRPC	Castration resistant prostate cancer
CTG	Cell Titer Glo
DAB	3,3'-Diaminobenzidine
DDR	DNA damage response
DMA	Dimethylacetamide
dMMR	Mismatch repair deficient
DNA	Deoxyribonucleic acid
DNA-PK	DNA-dependent protein kinase
DSB	Double strand breaks
EBRT	External beam radiation therapy
EC	Electron capture
EDC	1-Ethyl-3-(3-dimethylaminopropyl) carbodiimide
ELISA	Enzyme linked immunosorbent assay

EPR	Enhanced permeability and retention
eV	Electron volt
Fab	Fragment antibody binding
FBS	Fetal bovine serum
Fc	Fragment crystallizable
FcRn	Neonatal Fc receptor
FDA	Food and drug administration
FELASA	Federation for Laboratory Animal Science Associations
FGFR2	Fibroblast growth factor receptor 2
GC	Gastric cancer
H2A.X	H2A histone family member X
HER2	Human epidermal growth factor receptor 2
HMW	High molecular weight
HOPO	Hydroxypyridinone
HPGe	High purity germanium detector
HPLC	High-performance liquid chromatography
HR	Homologous recombination
IC_{50}	Half maximal inhibitory concentration
IgG	Immunoglobulin G
IRF	Immunoreactive fraction
iTLC	Instant thin layer chromatography
i.p	Intraperitoneal
i.v	Intravenous
LET	Linear energy transfer
mAb	Monoclonal antibody
MES	2-(N-morpholino) ethanesulfonic acid
MFI	Median fluorescence intensity
MSI	Microsatellite Instability
MSLN	Mesothelin
NER	Nucleotide excision repair
NET	Neuroendocrine tumors
NHEJ	Non-homologous end joining
NHL	Non-Hodgkin lymphoma

NHS	*N*-Hydroxysuccinimide
PARP	Poly (ADP-ribose) polymerase
^{207}Pb	Lead-207
PBS	Phosphate buffered saline
PEG	Poly-(ethyleneglycol)
PI	Propidium iodide
PIKK	phosphatidylinositol 3-kinase related kinase
p.o.	*Per os*, orally
^{223}Ra	Radium-223
RAC	Radioactive concentration
RBE	Relative biological effectiveness
RCP	Radiochemical purity
RIT	Radioimmunotherapy
ROS	Reactive oxygen species
RPA	Replication protein A
SSB	Single strand break
ssDNA	single strand DNA
TAT	Targeted alpha therapy
T/C	Treatment over control
^{227}Th	Thorium-227
TNBC	Triple negative breast cancer
TTC	Targeted thorium conjugate
XRCC1	X-ray repair cross-complementing protein 1

iii. List of Papers and Patents

Paper I

"Synergistic Effect of a Mesothelin Targeted Thorium-227 Conjugate in Combination with DNA Damage Response Inhibitors in Ovarian Cancer Xenograft Models", Published in *Journal of Nuclear Medicine*, March 8th 2019, DOI:10.2967/jnumed.118.223701.

Authors: Katrine Wickstroem, Urs B Hagemann, Véronique Cruciani, Antje M Wengner, Alexander Kristian, Christine Ellingsen, Gerhard Siemeister, Roger M Bjerke, Jenny Karlsson, Olav B Ryan, Lars Linden, Dominik Mumberg, Karl Ziegelbauer and Alan S Cuthbertson.

Poster at AACR Annual Meeting 2018; April 14-18, 2018; Chicago, IL: "Synergistic effect of MSLN-TTC in combination with DNA damage response inhibitors".

Paper II

"Preclinical Combination Studies of an FGFR2 Targeted Thorium Conjugate and an ATR Inhibitor BAY 1895344", manuscript submitted to *International Journal of Radiation Oncology, Biology, Physics.*

Authors: Katrine Wickstroem, Urs B Hagemann, Alexander Kristian, Christine Ellingsen, Anette Sommer, Heidrun Ellinger-Ziegelbauer, Uta Wirnitzer, Else-Marie Hagelin, Aasmund Larsen, Roger Smeets, Roger M Bjerke, Jenny Karlsson, Olav B Ryan, Antje M Wengner, Lars Linden, Dominik Mumberg and Alan S Cuthbertson.

Poster at AACR Annual Meeting 2018; April 14-18, 2018; Chicago, IL: "Increased in vitro potency and in vivo efficacy of FGFR2-targeted thorium-227 conjugate (FGFR2-TTC) in combination with the ATR inhibitor BAY 1895344".

Paper III

"Synergistic Effect of a HER2 Targeted Thorium-227 Conjugate in Combination with olaparib in a BRCA2 Deficient Xenograft Model", manuscript submitted to *Cancer Research*.

Authors: Katrine Wickstroem, Jenny Karlsson, Urs B Hagemann, Véronique Cruciani, Alexander Kristian, Roger M Bjerke, Olav B Ryan, Lars Linden, Dominik Mumberg, Michael Brands and Alan S Cuthbertson.

Poster at *Targeted-Alpha-Therapy* conference, 2019: "Synergistic Effect of a HER2 Targeted Thorium-227 Conjugate in Combination with olaparib in a BRCA2 Deficient Xenograft Model".

Patent

"Combination Therapy Comprising a radiopharmaceutical and a DNA-Repair Inhibitor".

Patent pending: WO 2018/153975 A1, August 30, 2018.

2 Abstract

The Targeted Thorium-227 Conjugates (TTCs) represent a novel class of cancer therapy currently in preclinical and clinical development at Bayer AS. The TTCs consist of the alpha emitter thorium-227 (^{227}Th) complexed to a 3,2-HOPO chelator conjugated to a tumor specific antibody. Since alpha particles release high energy over a short range they induce a potent local irradiation of the tumor with limited damage to surrounding tissue, thus making them beneficial for treatment of cancer.

This thesis describes the preclinical evaluation of TTCs in combination with DNA damage repair inhibitors. The DNA damage induced by the alpha-particle combined with inhibitors of DNA repair was hypothesized to result in synergistic effects as fewer double strand breaks (DSBs) per cell would be required to trigger cell death. The overall aim of the combination therapy is to increase the therapeutic window and improve the outcome of the treatment.

The experimental work summarizes the *in vitro* and *in vivo* studies exploring TTCs combined with the pharmaceutical or genetic inhibition of DNA damage response (DDR). First, the *in vitro* cytotoxicity and mechanism of action from the combination treatment was determined on a panel of cancer cell lines from different tissue origins. The *in vitro* screening confirmed that synergistic effects can be achieved over a range of cancer indications, targets and DDR inhibitors. Furthermore, the mechanistic studies demonstrated that the combination effect was in fact linked to downregulation of DNA damage repair. Based on results from the *in vitro* screening, combination therapy with the ATR inhibitor or PARP inhibitor was further explored in *in vivo* studies, evaluating the anti-tumor activity of TTC monotherapy and combination treatment in cancer xenografts in nude mice. The combination treatment demonstrated enhanced anti-tumor efficacy when combined with a non-efficacious dose of the inhibitor, with synergistic effect demonstrated for the ATR inhibitor in ovarian and breast cancer models and the olaparib combination resulting in additive effects in an ovarian cancer model.

In a final study, the effect of having a genetic knockout of the DNA damage response gene BRCA2 was evaluated, when exposed to combination therapy with PARP inhibitor and TTC. Both *in vitro* and *in vivo* it was demonstrated that the genetic knockout of BRCA2 sensitized to the TTC monotherapy as well as the combination therapy. Synergistic effect was only observed in the BRCA2 knockout model and not in the parental model that was used as comparison, thus reflecting the relevance of synthetic lethality for the combination therapy.

In summary, the work presented in the thesis demonstrates the rationale for combining TTCs with inhibition of DNA damage repair. As such, it supports the further exploration of TTCs in combination with DDR inhibitors for treatment of different cancer indications and investigation of defects in DDR genes as potential biomarkers for treatment with TTCs.

3 Background

3.1 The Principles of Radioimmunotherapy

Immunotherapy

The role of the immune system in both the development of cancer and as a tool for defeating the disease has been recognized for more than a century and therapeutic strategies for immune activation have become the fourth pillar of cancer therapy [1, 2]. Immunotherapy takes advantage of the intrinsic characteristics of the immune system to attack the tumor, including a wide range of approaches such as the use of immune cells, cytokines, cancer vaccines and antibodies to induce an anti-tumor effect [1].

Antibodies are plasma proteins, also called immunoglobulin (Ig), naturally produced and secreted from mature B-cells in response to bacterial or viral infections. Among the five subtypes of antibodies in humans (IgA, IgD, IgE, IgG and IgM), IgG are the most abundant of the plasma antibodies. IgG is a 150 kDa protein consisting of two identical heavy chains (2 x 50 kDa) and light chains (2 x 25 kDa) (see antibody structure Figure 1). The functionality of the antibody is largely linked to the antigen binding site which binds to specific epitopes on the pathogen, and an Fc-region binding to Fc-receptors on leukocytes or endothelial cells. The binding to Fc receptors on leukocytes initiates different immune responses, including Antibody dependent cell mediated cytotoxicity (ADCC), Complement dependent cytotoxicity (CDC) and Antibody dependent cellular phagocytosis (ADCP) [3]. The Fc-region of the antibody also binds to neonatal Fc-receptors (FcRn) on the surface of endothelial cells, leading to endocytosis and re-cycling rather than degradation in the lysosomes, a process which increases the blood half-life of the antibody.

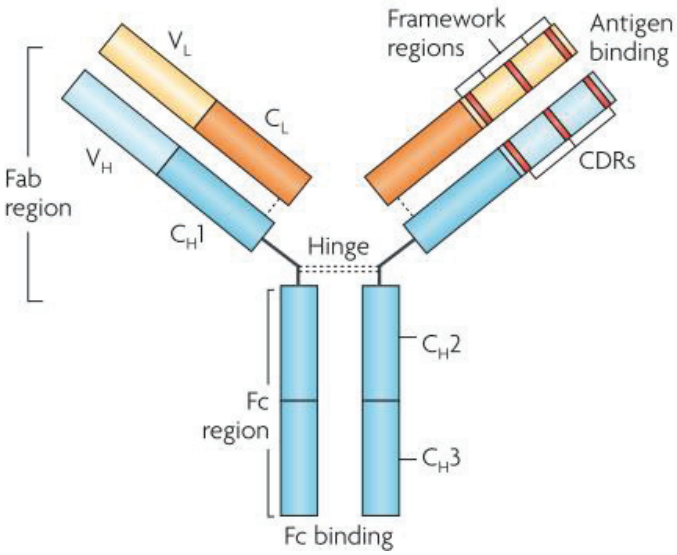

Figure 1 Schematic illustration of antibody structure. IgG antibodies consist of a fragment antigen binding (Fab) region with the antigen binding site and an Fc-binding region which binds to immune cells to elicit an immune response. Figure modified and re-printed from [4].

The IgG antibodies are attractive in therapy due to their ability to recognize and bind with high affinity and specificity to the target protein and their long half-life in blood permits infrequent dosing [4]. The discovery of the hybridoma technology presented by Köhler and Milstein in 1975 enabled the production of monoclonal antibodies (mAbs) revolutionizing the use in therapy [5]. Furthermore, to reduce the immunogenic mouse-component of the antibody the technology has gradually developed from production of mouse antibodies, to chimeric, humanized and finally fully human antibodies (Table 1) [4]. There are currently over 70 clinically approved therapeutic antibodies for treatment of various diseases such as arthritis, psoriasis, Crohn's disease and cancer [6]. The anti-cancer actions of therapeutic antibodies varies widely and includes mechanisms such as blocking or stimulation of signaling pathways and delivery of a cytotoxic payload specifically to the tumor via cell surface proteins on the cancer cells [7]. The targeted thorium conjugates (TTCs) described in this thesis are characterized as radioimmunotherapies (RITs) which take advantage of antibodies for the targeted delivery of ionizing radiation from the radionuclide thorium-227 to the tumor.

Table 1 Types of therapeutic monoclonal antibodies. Table modified from [4].

Antibody type	Structure	Antibody Nomenclature
Murine	Fully murine	o = mouse e.g. muro monab
Chimeric	Human constant + murine variable regions	xi = chimeric e.g. rituximab
Humanized	Murine complementarity determining regions (CDRs)	zu = humanized e.g. trastuzumab
Human	Fully human	u = human e.g. anetumab

Ionizing radiation in radioimmunotherapy

Radiation of more than 10 eV has enough energy to displace electrons from atoms and create ions, and is therefore characterized as ionizing radiation. In cancer therapy the aim of ionizing radiation is to create irreversible damage to the cancer cells which hinders the further proliferation of the tumor. Approximately 50 % of all cancer patients receive radiation therapy as part of their treatment, including x-rays, gamma rays and particle radiation [8]. In RIT a therapeutic antibody with high affinity for tumor antigens is exploited to achieve the delivery of a radioactive isotope to the tumor [9, 10]. In contrast to traditional external beam radiation therapy (EBRT), RIT is administered systemically to facilitate distribution to blood-borne cancers, local tumors as well as metastases, while sparing normal tissue. There are currently a range of different radioimmunoconjugates in pre-clinical and clinical studies [9]. The types of radioactive agents traditionally investigated and used for RIT includes alpha, beta and auger electron emitters (Table 2). RIT has so far been clinically approved with beta emitters for treatment of hematological cancers, including yttrium-90 labeled anti-CD20 ibritumomab tiuxetan (Zevalin®) and iodine-131 labeled tositumomab (Bexxar®), both indicated for treatment of non-Hodgkin lymphoma [11]. Furthermore, in addition to using antibodies, other targeting agents, such as antibody fragments are also being explored for the targeted delivery of radionuclides [9]. Radio-peptide targeted

therapy is already well established with radiolabeled somatostatin peptides, such as Lutathera®, being widely used in treatment of neuroendocrine tumors (NET) and peptidomimetics such as PSMA-617 used in compassionate use programs for the treatment of castration resistant prostate cancer [12]. Both approaches use the beta-emitter lutetium-177. The smaller size can be beneficial as it results in improved tumor penetration compared to IgG, in addition small molecules are excreted rapidly from the body very often by the renal excretion route, reducing side effects such as myelosuppression [9]. However, tumor retention with small molecules can often be a limiting factor. In addition, the fast clearance also decreases the time for target exposure which lowers the dose delivered to the tumor as compared to IgG [9].

The radionuclides used in RIT vary in their biological effectiveness depending on the type of ionizing radiation emitted. The term relative biological effectiveness (RBE) is often used to compare the effect of one type of radiation relative to another given equivalent levels of absorbed energy. The RBE is influenced by the absorbed dose, the dose rate, and the linear energy transfer (LET). The absorbed dose, measured in Gy, is the energy absorbed in matter per unit mass (1 Gy = 1 J/kg) and the LET is defined as energy released over a given distance in biological tissue (keV/μm) [13]. The beta emitters are categorized as low LET (0.2 keV/μm), auger as intermediate LET (4-26 keV/μm) and alpha is defined as high LET (50-230 keV/μm). The LET influences the type of DNA damage induced; see simplified illustration Figure 2. Low LET produces mainly sparse ionization events indirectly via the generation of reactive oxygen species (ROS) resulting in sublethal DNA damage. In contrast, high LET result in a broad ionization track in biological tissue and higher probability of inducing clustered double strand breaks (DSBs) involving two or more DSBs within one to two helical turns [14, 15]. The clustered DSBs are difficult for the cells to repair and therefore a higher RBE is assigned to the high LET alpha particles as compared to low LET such as gamma-rays, x-rays or beta-emitters [15, 16]. Thus, a lower radioactive dose is required when using alpha emitters to achieve the same cytotoxicity as for low LET [13].

Table 2 Radionuclides in Radioimmunotherapy. The table summarizes the characteristics of radionuclides currently used in clinical or pre-clinical studies. Two of the beta-emitters, yttrium-90 and iodine-131, are radionuclides used in approved RIT. Table adapted from [9].

Isotope	Half-life ($T_{½}$)	Maximum energy (keV)	Maximum range (μm)	Emission type
β-emitters (LET: 0.2 keV/μm)				
Yttrium-90	2.67 d	2280.0	11,300	β–
Iodine-131	8.02 d	606.31	2300	β–, γ
Lutetium-177	6.65 d	498.3	1800	β–, γ
Copper-67	61.83 h	577.0	2100	β–, γ
Rhenium-186	3.72 d	1069.5	4800	β–, γ
Rhenium-188	17.01 h	2120.4	10,400	β–, γ
Auger-emitters (LET: 4-26 keV/μm)				
Indium-111	2.80 d	26	17	Auger, γ
Gallium-67	3.26 d	9.6	3	Auger, β–, γ
Platinum-195m	4.02 d	64	76	Auger
Iodine-125	59.41 d	31.7	20	Auger, γ
α-emitters (LET: 50-230 keV/μm)				
Bismuth-213	45.59 min	8400	90	α, β–, γ
Bismuth-212	60.54 min	7800	100	α, β–, γ
Astatine-211	7.21 h	7500	80	α, EC
Actinium-225	9.92 d	8400	90	α, β–, γ
Thorium-227	18.7 d	7400	70	α, β–, γ

EC: electron capture

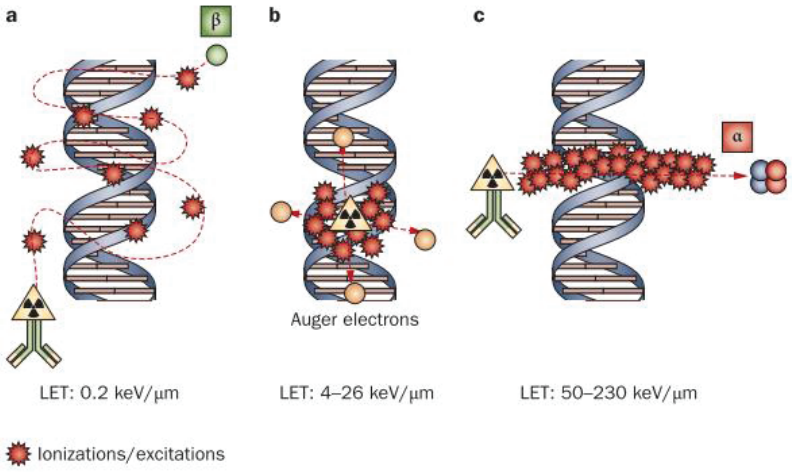

Figure 2 Comparison of DNA damage induced by radionuclides used in RIT a) beta emitters b) auger-emitters and c) alpha emitters. The different radioactive agents traditionally used in RIT can be categorized based on their linear energy transfer (LET), which affects the types of DNA damage produced and consequently the relative biological effectiveness (RBE). The low LET beta emitters produce sparse ionization events generating mostly single strand DNA damage. The auger electrons have intermediate LET and induce complex DNA damage, however the short range make them dependent on delivery into the cell in order to damage the DNA molecule. The alpha particles have high LET and induce mostly clustered DNA damage that is difficult to repair. Figure re-printed from [17].

3.2 Targeted Thorium Conjugates

In targeted alpha therapy (TAT) an alpha emitter is specifically delivered to the tumor via a targeting agent such as antibody, peptide or small molecule or simply by metabolic incorporation as in the case of radium-223 [18]. The alpha emitters release alpha particles, comprised of two neutrons and two protons. The alpha emitters are attractive for use in cancer therapy due to their high RBE and short range in biological tissue, which holds promise for potent and specific anti-tumor activity when delivered systemically to the tumor. This thesis describes the preclinical evaluation of targeted thorium conjugates (TTCs) comprising a cancer targeting antibody, a chelator moiety covalently conjugated to the antibody and the alpha particle emitting radionuclide thorium-227 (Figure 3). TTCs with different targeting antigens and indications are currently in pre-clinical and clinical development, including TTCs targeting CD22, CD33, CD70, FGFR2, HER2, MSLN and PSMA [19-23]. CD22-TTC, MSLN-TTC and PSMA-TTC are currently in phase I clinical trials, for the treatment of both hematological (CD22; NCT02581878) and solid tumor indications (MSLN; NCT03507452, PSMA; NCT03724747). In the following sections, the choice of the three building blocks compromising the TTC is explained.

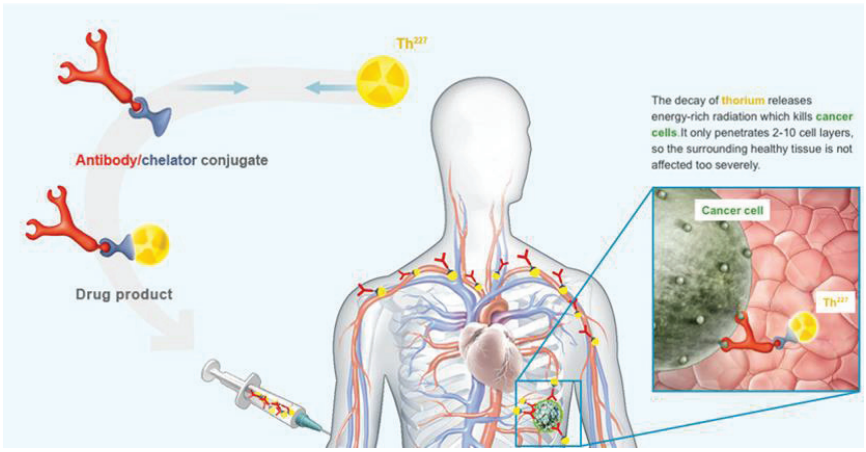

Figure 3 Targeted Thorium Conjugates. The TTCs consist of the alpha emitter thorium-227 (^{227}Th) coupled by a 3,2-HOPO chelator to a tumor specific antibody. The TTC is administered systemically and accumulate in the tumor based on binding to cancer-specific antigens, resulting in a potent and specific irradiation of the tumor while sparing normal tissue. Figure from Bayer AS.

The alpha emitter, thorium-227

The therapeutic advantage of alpha emitters has been recognized for more than a century and several alpha particle emitters are being explored as part of radioimmunoconjugates in preclinical and clinical studies, including actinium-225, astatine-211 and bismuth-213, see Table 2 [13, 18]. The first and only clinically approved alpha pharmaceutical Xofigo®, consisting of the alpha emitter radium-223, was approved for treatment of bone metastasis in castration resistant prostate cancer (CRPC) in 2013 [24]. Radium-223 targets bone metastasis based on its intrinsic ability to accumulate in bone. However, as radium-223 has not been successfully complexed to targeting agents, it is so far limited to treatment of bone disease. In contrast, thorium-227 forms stable complex with chelators and can therefore be used in radioimmunotherapy by connection to targeting moieties. Thorium-227 decays to stable lead-207 via a decay chain that generates five alpha particles, three beta particles as well as gamma emission that follows the alpha decay (Figure 4). The half-life of thorium is 18.7 days, which matches the half-life for antibodies in blood and also provides sufficient time to facilitate the production of the TTC followed by distribution and patient administration. Taken together, the thorium-227 is considered suitable for TAT based on its ability to form stable complex with chelators, its suitable half-life, and the availability for commercial production.

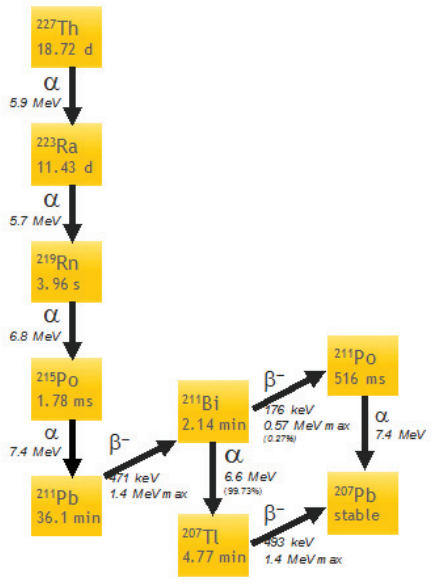

Figure 4 Thorium-227 Decay Chain. Thorium-227 (^{227}Th) is purified from an actinium-227 (^{227}Ac) generator and decays via its alpha and beta-emitting daughters to stable nonradioactive lead-207 (^{207}Pb). The alpha-emitting daughter, radium-223 (^{223}Ra), will detach from the antibody-chelator conjugate because of the substantial kinetic energy of the recoiling nucleus after the alpha particle emission. Figure from Bayer AS.

The 3,2-HOPO chelator

Non-efficient radiolabeling can result in the release of the radionuclide from the chelator, reducing tumor accumulation and increasing nonspecific uptake, affecting the efficacy and safety of the drug. Thus, much effort has been invested in the development of a chelator that is tailored for thorium-227, leading to the 3,2-hydroxypyridinone (3,2-HOPO) class [25]. As presented in Figure 5, the chelator consists of four N-methyl-3-hydroxy-pyridine-2-one metal binding units, a polyamine backbone and a linker containing a carboxylic acid group. The chelator binds thorium-227 rapidly and with high affinity and does not require heating; 20-30 minutes at room temperature is sufficient to achieve a stable complex. Recent studies have also demonstrated stronger binding of the thorium-227 as compared to other potential competing metal ions [26]. Furthermore, the carboxylic acid can easily be conjugated to an antibody via ε-amino groups of lysine residues in the antibody without affecting the binding properties of the antibody [19, 25].

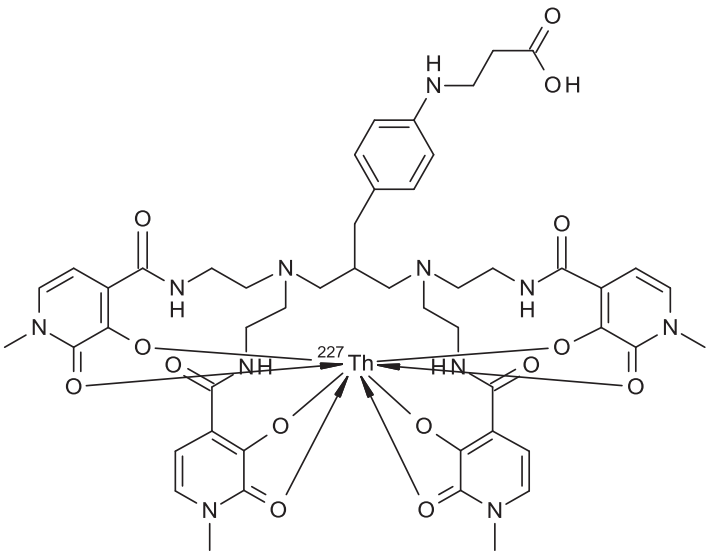

Figure 5 Chemical Structure of the 3,2-HOPO Chelator. Illustration of the 3,2-HOPO chelator and the complex formation with thorium-227. The carboxylic acid is conjugated to the antibody via ε-amino groups of lysine residues in the antibody. Figure from Bayer AS.

The monoclonal antibodies

The characteristics of both the cancer target and the monoclonal antibodies are important factors influencing the efficacy and safety of the drug [4]. Ideally the antigen target should be over-expressed in the tumor or tumor microenvironment, with low expression in normal tissue to minimize adverse effects. This thesis describes TTCs targeting three different tumor associated antigens, fibroblast growth factor receptor 2 (FGFR2), mesothelin (MSLN) and human epidermal growth factor receptor 2 (HER2), as summarized in Table 3, and the respective antibodies summarized in Table 4. Common for all targets is the overexpression in multiple cancer indications, minimal expression in normal tissue and a link to poor prognosis for patient survival [27-29]. HER2 and FGFR2 are growth factor receptors, while the function of MSLN is not fully understood, although it has been suggested to involve cell adhesion [30]. All antigen targets have demonstrated antigen shedding, which should be taken into consideration during potential clinical studies as the biodistribution of the drug may be affected. In addition, many mAbs are internalized upon binding to antigen target and although this may contribute to potency of the TTCs, due to the path length of the alpha particle, it is not prerequisite for efficacy.

The antibody component of MSLN-TTC, anetumab, is a fully human IgG1 antibody that has previously been shown to be highly effective in inhibiting tumor growth in MSLN expressing tumors in an ADC format (anetumab ravtansine, BAY 94-9343) and is currently being evaluated in clinical studies (NCT02610140) [31]. The FGFR2-TTC contains the fully human IgG1 BAY 1179470 which has also demonstrated specific efficacy in pre-clinical studies using an auristatine-based ADC [32]. The FGFR2 antibody is the only antibody presented in the thesis which is cross-reactive to murine antigen, with a similar K_D-value to the human target, making it possible to evaluate the normal-tissue distribution in mice.

The antibody used in the HER2-TTC is the humanized IgG1 antibody, trastuzumab. The HER2 target, in contrast to FGFR2 and MSLN, is already extensively used in the clinic for targeted cancer therapy [33]. In 1998, trastuzumab (Herceptin®) was the first HER2 targeting drug approved by FDA. It was approved for treatment of metastatic breast cancer with HER2 overexpression and later also gastric cancer. Since then, also pertuzumab (Perjeta®), the antibody drug conjugate (ADC) Ado-trastuzumab-emtasine (Kadcyla®) and the small molecule HER2-inhibitor lapatinib (Tyverb®) have been approved for HER2 positive breast cancer [28]. However, these therapies are limited as patients commonly experience either intrinsic or developed drug resistance. In the case of trastuzumab, pertuzumab and lapatinib, the drug resistance is often related to upregulation of downstream signalling pathways or mutations in HER2 that affects binding of the antibodies [33, 34]. In the case of the ADC, Kadcyla®, the resistance mechanisms can in addition be linked to the over-expression of drug efflux pumps or poor internalization, both leading to insufficient uptake of the cytotoxic agent [35]. Due to the high energy and physical destruction caused by the alpha particle, activity from TTC is still expected in the resistance setting provided the epitope on HER2 is unaffected.

Table 3 Characteristics of Tumor Antigens

	FGFR2 (Fibroblast growth factor receptor 2)	**HER2** (Human epidermal growth factor receptor 2)	**MSLN** (Mesothelin)
Normal protein function	Proliferation and growth [36]	Proliferation and growth [28]	Cell adhesion [30]
Cancer indications with target overexpression	Breast Colorectal Gastric Lung [36]	Breast Colon Gastric Lung Ovarian Pancreas [33]	Mesothelioma Lung Ovarian Pancreas TNBC [29, 37]
Antigen shedding	Antigen shedding demonstrated *in vitro* [38]	Yes [39]	Yes [40]

Table 4 Characteristics of Antibodies

	FGFR2-mAb/ BAY 1179470	HER2-mAb/ Trastuzumab	MSLN-mAb/ Anetumab
Structure	Fully human IgG1 antibody	Humanized IgG1 antibody	Fully human IgG1 antibody
Binding affinity, Kd (nM)*	75	5	14
Murine/ cynomologus cross reactivity*	Yes/ Yes	- / Yes	- / -
Internalization	Yes [32]	Yes [41]	Yes [31]
Approved drugs	-	Herceptin® Kadcyla ®	-

* Internal data

3.3 Radiobiological Effects

The radiobiological effects describe the cellular consequences after treatment with ionizing radiation, including cellular damage, activation of signaling pathways, cell cycle arrest, DNA damage repair and cell death mechanisms [17].

The DNA Damage Response

Due to its chemical composition, complex structure and critical role in cellular function, the DNA molecule is the major target for ionizing radiation in cancer therapy [15]. Ionizing radiation induces a range of different DNA damage, such as base damage, base loss, DNA-protein crosslinks, single strand breaks, double strand breaks and clustered DNA lesions [42]. However, as the cell is naturally exposed to DNA damaging agents both externally and from endogenous oxidative metabolism, it has developed complex mechanisms to detect and repair different types of lesions [43]. The DNA damage response (DDR) involves a network of proteins. DNA damage triggers the activation of sensor kinases, ATR, ATM and DNA-PK, which phosphorylate histone proteins (H2A.X) close to the site of the damage, further activating proteins involved in cell cycle arrest and DNA repair. The main types of repair initiated by ionizing radiation includes single strand DNA repair, including base excision repair (BER), nucleotide excision repair (NER) and double strand DNA damage, mainly non-homologous end joining (NHEJ) and homologous recombination (HR) [44].

The choice of DSB repair is determined by the cell cycle phase, complexity of the damage and availability of co-factors [45]. In HR, the cell uses the sister chromatid for repair, this mechanism can therefore only occur when the cell has an available sister chromatid during the late-S- and G2-phase [46]. While for NHEJ, the two blunt ends are re-joined directly without using a template. This makes it a more error-prone mechanism, however enabling DSB repair in the different phases of the cell cycle [47]. The capacity to repair the DSB is critical as only a single DSB can be lethal to the cell [48]. This is also reflected by the varying radiosensitivity of the cell cycle phases which is affected by the cells ability to facilitate DSB repair in the different phases [49]. The final result following the DNA damage response is either survival or cell death depending on the severity of the damage and the genetic makeup of the cancer cell.

Cell death due to ionizing radiation

If the damage is too severe to be repaired properly the normal cellular response is to initiate programmed cell death a process known as apoptosis. However, cancer cells commonly have defects in the apoptosis program, frequently due to loss of function or mutations in genes such as TP53, BAX and BCL-2 [50]. For example, it has been reported that over 50 % of cancer patients have mutations in the tumor suppressor gene TP53 [51], which has also been demonstrated to be essential for radiation induced apoptotic cell death [52]. As such, the high frequency of defects in the apoptosis program, typically allows the cell to continue to divide and other types of cell death such as mitotic catastrophe, autophagy and necrosis are more dominant following treatment with ionizing radiation including alpha particle radiation [53, 54].

Off-target effects from ionizing radiation

Both local and systemic off-target effects may also influence treatment outcome following ionizing radiation. Radiation-induced bystander effects are local responses involving signaling from the irradiated cells to nearby cells that are not traversed by the radiation. The effect was first discovered based on the observation that ionizing radiation was determined to be lethal also to

non-irradiated adjacent cells [55]. It was later determined that the bystander effect involves GAP junctions or soluble signaling molecules and the response can vary between activation of cell death receptors to activation of growth receptors depending on the cell type and the LET of the radiation [55]. In contrast, the abscopal effect is a systemic effect demonstrated after irradiation. It was first described in 1953 as a radiobiological phenomenon involving tumor response at a distance site from where the tumor was locally irradiated [56, 57]. The mechanisms for the abscopal effect were partially explained firstly in 2004, with emerging evidence that the immune system was involved providing a vaccination effect [58]. Alpha particle radiation has been demonstrated to induce immunogenic cell death, antigen-specific T-cell response and off-target effects, indicating involvement of the immune system in response to alpha therapy [59]. As such, immune activation is also expected to be a critical component of the mechanisms underlying responses to TTC therapy.

3.4 Modification of DNA Damage Response

In traditional radiobiology the five R's are typically used to describe the effect and outcome of radiotherapy; Repair of DNA damage, Redistribution in cell cycle, Re-oxygenation of tumor tissue, Repopulation of cancer cells following treatment and the intrinsic Radiosensitivity of the tissue type [60]. The focus of this thesis has been to investigate the effect of inhibiting different DNA repair mechanisms. The DNA damage response is an important influencer of both the development of cancer and the response to treatment. Firstly, DDR genes are frequently mutated in cancer. This typically involves defects in tumor suppressor genes in the early stage of cancerogenesis allowing for the proliferation of aberrant cells which may further trigger chromosomal instability [61]. Therefore, certain hereditary DDR mutations such as defects in the HR genes BRCA1 and BRCA2, or mismatch repair genes MSH2 and MLH1 predispose an individual for the development of cancer [62, 63]. Furthermore, cancer cells can also exploit the DDR program to enhance survival following cancer therapy or develop mechanisms of resistance by upregulation of genes linked to DDR [64].

On the other hand, it is also possible to exploit these differences between the cancer and the normal tissue in the development of targeted agents. The concept known as synthetic lethality, takes advantage of defects in the cancer cells to differentiate the treatment response between normal tissue and the tumor, thereby creating selectivity [47, 65]. Thus, based on the importance of DDR, there are several cancer therapies being explored, both as monotherapies as well as in combination with DNA damaging agents such as chemotherapy and radiotherapy [47]. In this thesis different inhibitors, previously shown to have radiosensitizing effect with low LET radiation, are explored in combination with TTCs. Due to the high LET, RBE and complex nature of the damage induced by alpha particles it is generally considered that there would be less of a potency gain through combinations as compared to low LET [13]. However some pre-clinical studies have previously demonstrated enhanced effect of alpha therapy combination with inhibitors of DDR, including the genetic inhibition through knockdown of BRCA1 or pharmaceutical inhibition of DNA-PK combined with bismuth-213 labeled anti-EGFR antibody cetuximab (Erbitux®) [66, 67]. The studies presented in this thesis include inhibitors of the sensor kinases ATM, ATR and DNA-PK which are central in repair of DNA double strand damage and PARP1/2, involved in repair of single strand DNA damage (Figure 6).

The first clinical examples of efficacy through synthetic lethality in cancer therapy were the PARP inhibitors. Poly ADP ribose polymerase 1 (PARP1) and Poly ADP ribose polymerase 2 (PARP2) are nuclear enzymes, centrally involved in base excision repair (BER) [68] (Figure 6A). PARP1 detects single strand breaks (SSBs), triggering it to add poly (ADP-ribose) polymers to itself and surrounding histone proteins (poly ADP ribosylation) [69]. The modification leads to the recruitment of DNA repair proteins, including APE1, XRCC1 and DNA ligase III, which will further activate BER. PARP2 is closely related to PARP1, share common binding partners and cooperates with PARP1 in BER [70].

The PARP inhibitor is competing for substrate binding with NAD+ and thereby prevents poly ADP ribosylation and BER [71]. The inhibition of PARP therefore leads to accumulation of DNA damage and higher dependency on remaining DNA repair pathways. Furthermore, the inhibition of PARP combined with gamma radiation has previously demonstrated upregulation of G2 cell cycle arrest and downregulation of G1 cell cycle arrest, also indicating a role in cell cycle checkpoint mechanisms [72, 73]. In the studies presented in this thesis the FDA approved PARP1/2 inhibitor olaparib (Lynparza®) was used, which is administered as a single agent in BRCA mutated ovarian and breast cancer. BRCA1 and BRCA2 are tumor suppressor genes with protein products that play important roles in DNA double strand repair by facilitating the recruitment of RAD51 to the replication protein A (RPA)-coated single strand DNA (ssDNA), which is an essential step for HR (Figure 6B). BRCA deficient cells have demonstrated increased sensitivity to PARP inhibition compared to normal cells, with 57-fold difference for BRCA1 and 133-fold difference for BRCA2 [74] and the PARP inhibitor works efficiently in patients characterized with germline BRCA mutations [75]. The inhibition of PARP activity leads to the accumulation of DSBs and a higher dependency on the compensating BRCA proteins. In addition to the lack of catalytic activity of PARP, other mechanisms for synthetic lethality have also been proposed including that the trapping of the PARP enzyme on the DNA strand is inducing a cytotoxic effect [76].

ATR, ATM and DNA-PK are serine-threonine kinases that are members of the phosphatidylinositol 3-kinase related kinase (PIKK) family, which share extensive sequence homology and are all DNA damage sensors with central roles in DSB repair [61, 77] (Figure 6B). Due to the homology between the members of the PIKK family, the development of pharmaceutical for these targets have been challenged with lack of selectivity and high toxicity, which has hindered the further development of the drug [61]. As such, the selectivity to target was an important consideration for the choice of inhibitors in the studies presented.

The Ataxia-telangiectasia mutated (ATM) kinase is activated and recruited to DSBs by the MRE11-RAD50-NBS1 (MRN) complex. In response, ATM phosphorylates several substrates, including histone proteins H2A.X, which enables the recruitment of DDR proteins to the damage site and further activation of different pathways. This involves activation of the transcription factor P53, which will further activate genes involved in apoptosis, G1 cell cycle arrest and senescence [78] and Chk-2 leading to activation of intra-S-phase checkpoint [79]. In addition, ATM is involved in DSB repair via BRCA1 which promotes HR [80] and 53BP1 which stimulates NHEJ [81](Figure 6). The balance between BRCA1/53BP1 has been described to influence the choice of DSB repair mechanism [82]. Similarly to TP53, ATM is also a tumor suppressor gene known to be mutated in several cancer indications [83]. The complete loss of ATM function seen in the hereditary disorder ataxia-telangiectasia (A-T), causes high sensitivity to ionizing radiation [84], which has triggered the pharmaceutical development of ATM inhibitors as sensitizers to DNA damaging agents [61]. The studies presented in this thesis included the ATM inhibitor (ATMi) AZD0156, which is a specific and potent inhibitor of ATM that is currently in clinical phase I trials both as monotherapy and in combination with olaparib and irinotecan in patients with advanced cancer (NCT02588105).

Ataxia telangiectasia and Rad3 related (ATR) is activated by different types of DNA damage including DSBs and errors derived from interference with DNA replication and increased replication stress [85]. ATR is recruited to RPA-coated ssDNA via ATRIP, leading to the activation of ATR kinase, which will via downstream targets, including Chk1, activate cell cycle arrest in G2/M transition and intra-S-phase, DNA repair and restart of stalled replication forks [61]. Inhibition of the ATR kinase has therefore been proposed as an anti-cancer therapy in tumors characterized with increased DNA damage or repair deficiencies, high replication stress or in combination therapy with DNA damaging agents [61, 86]. Due to the partially overlapping function of ATR and ATM [87], defects in the ATM pathway have been demonstrated to sensitize to ATR inhibitors, presenting the potential for synthetic lethality in treatment with ATRi [88, 89]. Furthermore, several studies have

demonstrated the radiosensitizing effect of the ATR inhibitors with low LET radiation [61, 90]. In the studies presented the novel ATR inhibitor (ATRi) BAY 1895344 was used, which has shown high selectivity for the ATR kinase and is currently in clinical phase I, indicated for advanced solid tumors and lymphomas (NCT03188965).

The DNA-dependent protein kinase (DNA-PK) is in addition to being a DNA damage sensor kinase activated by DSBs, is also a key protein in NHEJ. DNA-PK is activated and recruited to DSBs by Ku70/80 bound to DNA. This will further lead to recruitment of proteins that ensures ligation of the two broken DNA ends, including XRCC4 [91] and DNA ligase IV [92]. Pre-clinical studies have previously demonstrated the radiosensitizing effect of DNA-PK inhibitors including combinations with alpha emitters [66, 67, 93]. Interestingly, the radiosensitizing effect of cetuximab, which is currently being used clinically in combination with radiotherapy [94], has been linked to the downregulation of downstream DNA-PK and ability to repair DNA damage [95]. The DNA-PK inhibitor (DNA-PKi) VX-984 was used in the studies presented [93]. This inhibitor is selective for DNA-PK and is also currently in clinical studies in combination with PEGylated liposomal doxorubicin indicated for advanced solid tumors and lymphomas (NCT02644278).

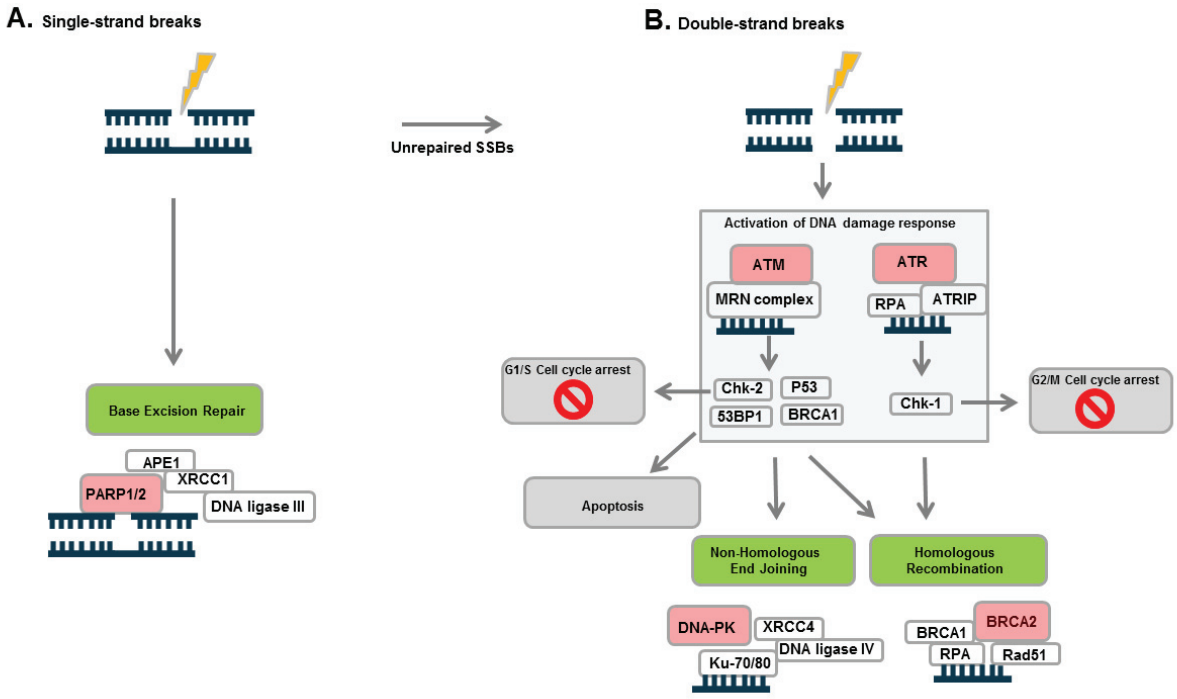

Figure 6 Key pathway components in DNA damage response initiated by single strand breaks (SSBs) and double strand breaks (DSBs). The DDR proteins targeted in the thesis are shown in red boxes and the different DNA repair mechanisms in green boxes. **A.** SSB repair. PARP1 and PARP2 are nuclear enzymes, centrally involved in BER by detecting single strand DNA breaks and recruiting repair proteins to the damage site. **B.** DSB repair. ATM, ATR and DNA-PK detect DSBs and activate DNA damage response which includes initiation of cell cycle arrest, DSB repair and apoptosis. ATM is considered principal mediator of G1/S cell cycle arrest, in contrast to ATR which mediates G2/M cell cycle arrest. NHEJ and HR represent the two main repair mechanisms for DSBs.

4 Aim of Project

The aim of the PhD project was to explore the *vitro* and *in vivo* effect of inhibiting DNA damage response in combination with TTC treatment. The thesis summarizes three preclinical studies involving both pharmaceutical and genetic inhibition of DNA damage response in combination with three novel TTCs (Table 5). The work included DDR inhibitors of both single strand DNA and double strand DNA damage repair, as these are common defects in response to ionizing radiation. The relevance of carrying genetic defects in DNA damage response both with respect to the monotherapy with TTCs as well as combination effect with DDR inhibition was also explored.

Table 5 Aim of Study

Study	Scientific questions
1.	1. *In vitro* screening of DDR inhibitors in combination with MSLN-TTC – Establish a suitable screening method – Does MSLN-TTC synergize with DDR inhibitors? 2. Mechanistic studies of synergistic combinations – Does the combination increase level of DSBs? 3. Establish suitable model to evaluate combination effect *in vivo* – What dosing regimen of MSLN-TTC is suitable for combination therapy? Does MSLN-TTC induce DSBs *in vivo*? 4. Evaluate combination *in vivo* effect based on *in vitro* screening – Is the *in vitro* synergy translatable to an *in vivo* setting? Is it possible to achieve enhanced effect at lower radioactivity levels?
2.	1. Evaluation of FGFR2 as a novel TTC target – Is FGFR2-TTC inducing specific anti-cancer activity on FGFR2-expressing cell lines *in vitro* and *in vivo*? 2. Biodistribution FGFR2-TTC in nude mice 3. Mechanistic studies of synergistic combinations – Does the combination increase level of DSBs? How does the combination affect the cell cycle arrest given the critical role of the ATR kinase in G2/M cell cycle arrest? 4. Evaluation of combination effect *in vivo* – Is the *in vitro* synergy translatable to an *in vivo* setting? Is it possible to achieve enhanced effect at lower radioactivity levels?
3.	1. Evaluation of *in vitro* cytotoxicity of HER2-TTC ± PARPi olaparib in BRCA2 deficient cell line as compared to BRCA2 functional cell line 2. Evaluation of biodistribution of HER2-TTC in HER2-low expressing model *in vivo* – Can specific uptake of HER2-TTC be achieved despite low HER2 tumor expression? 3. Evaluation of the *in vivo* effect of HER2-TTC ± PARPi olaparib – Does the BRCA2 knockout sensitize to TTC monotherapy? – Does the combination induce synergistic effect *in vivo*? Is it possible to achieve enhanced effect at lower radioactivity levels? – Does the combination effect differ between the BRCA2 knockout/BRCA2 functional models?

5 Experimental Methods

5.1 Conjugation

The conjugation procedure was achieved through *in situ* activation of the chelator using EDC/NHS chemistry followed by incubation with the antibody in PBS, as presented in Figure 7.

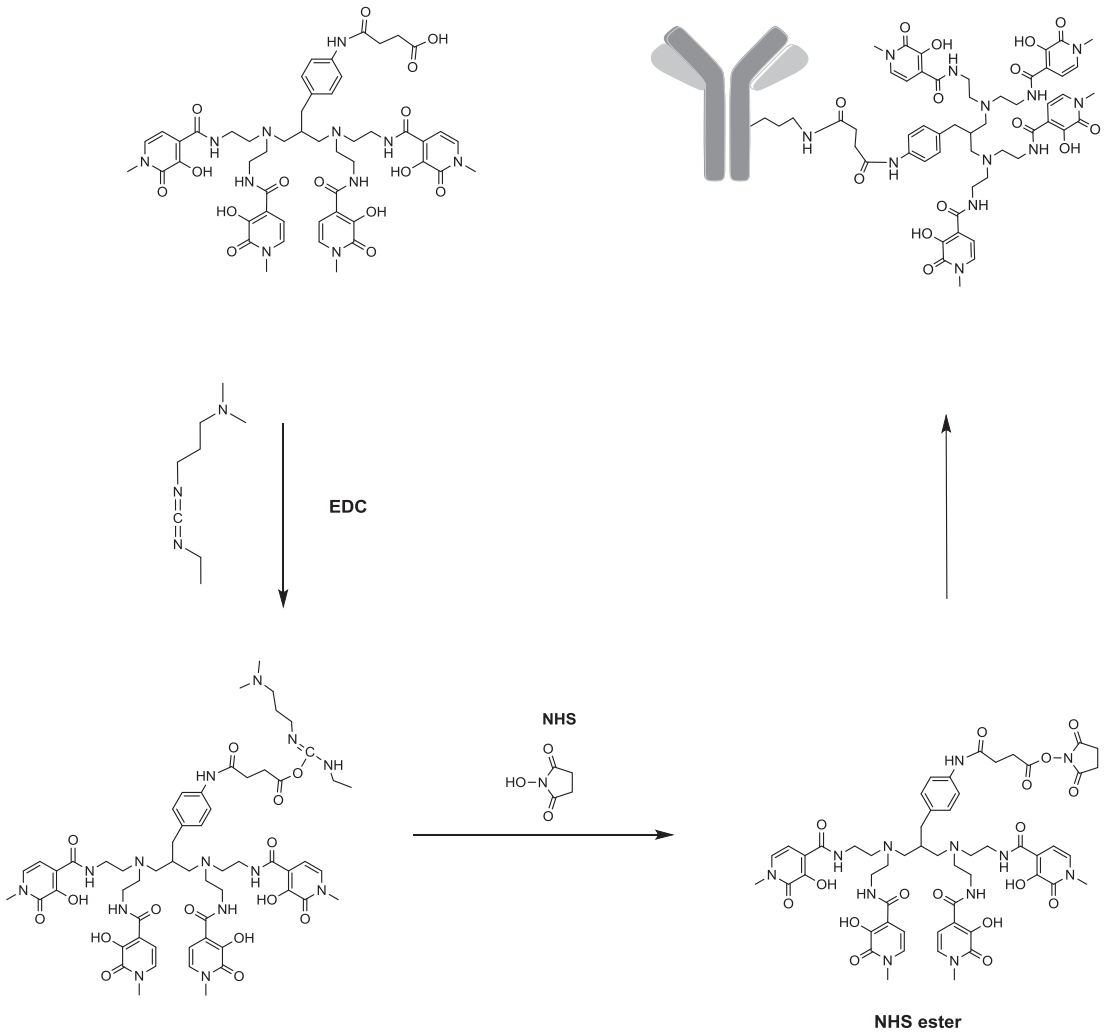

Figure 7 Conjugation Reaction, Coupling the 3,2-HOPO Chelator to the Antibody. EDC is activating the carboxyl group of the chelator to form a highly reactive intermediate, which further reacts with NHS to form NHS ester. The resulting NHS ester reacts with e-amino groups of lysine residues of the antibody to form the stable amide bond. Figure from Bayer AS.

Procedure: 1-Ethyl-3-(3-dimethylaminopropyl) carbodiimide (EDC) (Thermo Scientific, Cat# PG82079) and *N*-Hydroxysuccinimide (NHS) (Sigma Aldrich, Cat# 130672-5G) were dissolved to 10 mg/ml in 0.1 M 2-(N-morpholino) ethanesulfonic acid (MES) buffer at pH 5.5. The chelator was dissolved to 10 mg/ml in 0.1 M dimethylacetamide (DMA): MES (1:1) buffer at pH 5.5. The chelator solution (chelator/NHS/EDC) was activated for 30 min shaking at 750 rpm at room temperature in the dark, followed by incubation with antibody in PBS, pH 7.0, for 60 min at room temperature.

The chelator-to-antibody ratio (CAR) was determined by size exclusion chromatography (SEC) (TSKgel SUPER SW 3000 column; Tosoh Bioscience) by monitoring the absorbance of the antibody-chelator conjugate, with detection of mAb at 280 nm and chelator at 335 nm. The CAR value was calculated using the following formula:

$$CAR = \varepsilon\,\text{mAb}\,(335\text{ nm}) - \left[\frac{\text{R x }\varepsilon\,\text{mAb}\,(280\text{ nm})}{\text{R x }\varepsilon\,\text{chelator}\,(280\text{ nm})}\right] - \varepsilon\,\text{chelator}\,(335\text{ nm})$$

with ε mAb being the extinction coefficient of the antibody at 335 nm or 280 nm, ε chelator being the extinction coefficient of the chelator at 335 nm or 280 nm and R being the 335 nm to 280 nm area ratio of the antibody-chelator conjugate monomer determined from the SEC chromatograms.

5.2 Radiolabeling of Antibody Conjugate

Thorium-227 was purified from an actinium-227 generator [96]. Antibody-chelator conjugates were mixed with thorium-227 activities ranging from 0.5 – 2.5 MBq and incubated at room temperature for 60 min. Radiochemical purity (RCP), defined as the amount of thorium-227 bound to the TTC, was determined by instant thin-layer chromatography (iTLC).

5.3 Characterization of TTC

After radiolabeling the TTCs are characterized for binding affinity and radiostability using enzyme linked immunosorbent assay (ELISA), determination of immunoreactive fraction (IRF) and high-performance liquid chromatography (HPLC).

For ELISA, recombinant human MSLN/FGFR2/HER2 was coated to 96-well plates (1 µg/mL; NUNC/Maxisorp). Wells were blocked with 3 % BSA in PBS. Cold antibody conjugate, an isotype control antibody and the radiolabeled TTC were titrated on an ELISA plate pre-coated with the TTC-target. Unbound samples were washed off and bound samples were visualized using horseradish peroxidase labeled goat anti-human lambda antibody (Southern Biotech) followed by visualization with the peroxidase substrate ABTS (Life Technologies). The absorbance was measured at 405 nm in a plate reader (Perkin Elmer). EC_{50} values were calculated using GraphPad Prism Software.

In the FGFR2 study determination of the IRF and radiostability testing by radio-HPLC was also evaluated as part of the general assessment of a new TTC. The IRF was determined according to Lindmo [97] and performed as follows: recombinant human FGFR2-Fc or BSA was coated to tosyl-activated magnetic beads (Dynabeads M-280; Thermo Fisher Scientific). Fifty Becquerel of FGFR2-TTC/sample was incubated for 2h at 37°C using a titration of 4500 to 10 million beads coated with either FGFR2-Fc or BSA. Beads were sorted on a magnetic rack and the radioactivity in supernatant and on bead pellets was determined. The IRF was calculated as the fraction of activity bound to FGFR2-coated beads subtracting the activity measured on BSA-coated beads. For radiostability testing, the FGFR2-TTC was analyzed at 48 hours post reconstitution on a radio-HPLC equipped with a gamma radiation detector using a SEC column (TSKgel SUPER SE 3000; Tosoh Bioscience).

5.4 Preparation of DDR Inhibitors

ATRi BAY 1895344 (2-[(3R)-3-methylmorpholin-4-yl]-4-(1-methyl-1H-pyrazol-5-yl)-8-(1H-pyrazol-5-yl)-1,7-naphthyridine) was identified and synthesized at Bayer AG (WO2016020320 [98]). PARPi (olaparib), ATM inhibitor (AZD0156) and DNA-PK inhibitor (VX-984) were synthesized at Bayer AG. For *in vitro* studies, small molecule DDR inhibitors were dissolved in 100% DMSO (dimethyl sulfoxide) and further diluted in cell culture medium as indicated. For *in vivo* studies, BAY 1895344 was formulated in a vehicle consisting of 60% PEG400 (polyethylene glycol 400), 10% ethanol and 30% water at pH 7–8, olaparib was formulated in PBS supplemented with 10% 2-HPβCD ([2-Hydroxypropyl]-β-cyclodextrin).

5.5 Receptor density measurements

All cell lines included in the thesis were evaluated for the receptor density of the respective TTC antigen target. Cells were seeded in 96 well plates (100 000 cells, 100 µl) and incubated with a titration of 0.0006-100 µg/ml of anti-MSLN/HER2/FGFR2 antibody for one hour at 4°C, followed by incubation with 100 µl anti-human IgG-PE (Cat# 409304, Biolegend) for one hour at 4°C. The mean fluorescence intensity (MFI) was calculated using GraphPad Prims software version 7.0 and was plotted against the protein concentration. The mAbs/cell was determined making a standard curve using beads from Quantibrite (BD biosciences).

5.6 Cytotoxicity Assays

For evaluation of the combination effect cell lines and TTC/DDRi combinations were screened using the isobologram assay. The effect from the combination treatment was compared to the individual effect by plotting the IC_{50} values in an isobologram and calculating the combination indexes. The isobologram, shown in Figure 8, is a diagram that indicates if the different concentrations of the compound mixtures give an additive, synergistic or antagonistic effect [99]. The combination index

provides a quantitative estimation of the extent of synergy or antagonism, enabling the comparison among different cell lines and inhibitors used.

Procedure: Cells were seeded in 384 well plates and treated with a titration of TTC and DDRi's using a D300e digital dispenser (Tecan). The compounds were dispensed by titration in the following combination ratios with TTC (C1) and the DDRi (C2): 1xC1, 0.9xC1+0.1xC2, 0.8xC1+0.2xC2, 0.7xC1+0.3xC2, 0.6xC1+0.4xC2, 0.5xC1+0.5xC2, 0.4xC1+0.6xC2, 0.3xC1+0.7xC2, 0.2xC1+0.8xC2, 0.1xC1+0.9xC2 and 1xC2. Thus, the experimental setup comprises in total 11 titrations, with varying dose fractions of TTC and the inhibitors. Cell viability was determined by use of CellTiter-Glo® Luminescent Cell Viability Assay (Promega) according manufacturer's protocol. The absolute IC_{50} values were determined by using GraphPad Prism software version 7.0. The IC_{50} isobolograms were generated by plotting the actual IC_{50} values of TTC and DDRi along the x- and y-axis, respectively. The combination index (CI) was determined according to the median-effect model of Chou-Telalay [100], with CI<0.8 defined as synergistic effect, 0.8≤CI≤1.2 defined as additive effect and CI>1.2 defined as antagonistic effect.

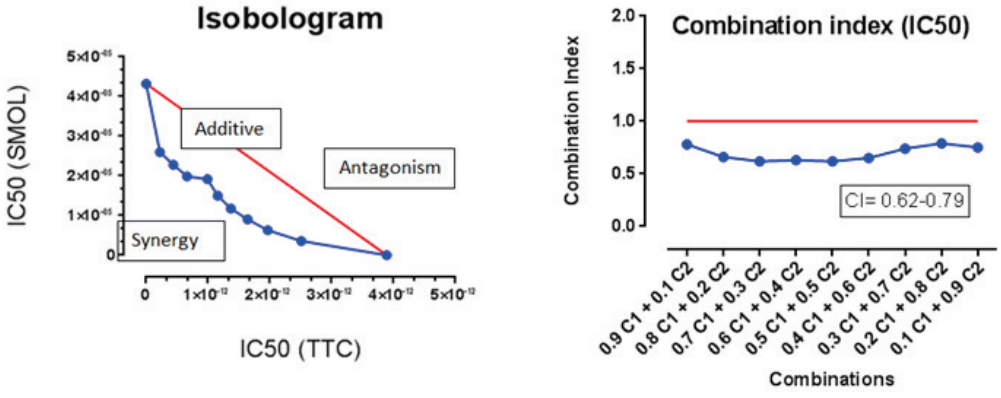

Figure 8 Example of Isobologram and combination index plot. As indicated in the text boxes: points over the red line indicates antagonism, points under the red line indicates synergy and points along the red line indicates additive effect. Figure from Bayer AS.

5.7 Mechanistic Studies

The mechanistic studies included determination of γH2A.X, cell cycle arrest and apoptosis.

Within seconds after induction of DSBs, the sensor kinases will phosphorylate the histone versions H2A.X nearby the damage site to thereby initiate cell cycle arrest and DNA repair. The phosphorylated version of H2A.X is often abbreviated γ-H2A.X and is a common target for determining DSBs [101]. Although this is an early marker, the effect from TTC is typically not seen until 2-3 days as the thorium-227 (t ½: 18.7 d) must have time to decay before DNA damage can be observed. As such, DSBs was determined after three days incubation with TTC ± inhibitor. Cell cycle arrest can be evaluated by determining the DNA content in the cell, since the cells have double amount of DNA in G2/M phase compared to G1 phase they appear as two separate colonies when stained and measured for DNA. Note: a mitosis marker was not included in the cell cycle analysis, cells in mitotic phase and G2 phase can therefore not be distinguished. Thus, cells with 4N DNA content are labeled G2/M.

If the cell is not able to repair the DNA damage it may initiate apoptosis. This is a form of programmed cell death that includes a cascade with caspase signaling, DNA condensation, DNA fragmentation and formation of apoptotic bodies. Caspase 3 is activated in the apoptotic cells both for the intrinsic and extrinsic apoptotic pathways. Cleaved caspase-3 is the activated version and can be used as a marker for apoptosis. In addition to determining the level of apoptosis as a marker for cell death, we also use this marker to exclude cells where the apoptotic DNA fragmentation process has started from our γH2A.X positive cells.

Procedure: Cells were seeded in 12 well plates (2 ml/well) or 6 well plates (4 ml/well) the day before start of treatment. The test compound was added to the cells, after three days exposure the cells were fixed with 70 % ethanol, followed by intracellular staining and detection with flow cytometry (Guava Easycyte 8HT). For cell cycle analysis, the cells were stained with PI/RNase (Cat#

F10979, Thermo Fisher). For detection of DNA double strand breaks, the cells were stained with phospho-Histone H2A.X (γH2A.X) (Ser139) antibody (Alexa Fluor® 647 Conjugate, Cat# 9720, Cell Signaling Technology). Cleaved caspase 3 (Asp175) antibody (Cat# 9669 Alexa Fluor® 488 Conjugate, Cell Signaling Technology) was used to exclude apoptotic cells and the % γH2A.X-positive cells were determined by gating using the population of control cells. The data analysis was performed using FlowJo software (version 10). Bar charts were created using GraphPad Prism software (version 7).

5.8 *In vivo* Studies

Animal Models

For all animal studies reported in this thesis we have used nude mice. The nude mice contain a mutation resulting in the lack of a functioning thymus which leads to the absence of or a very limited level of T-cells. This in turn, results in a reduced immune system, enabling the growth of human xenograft models without rejection of the tumor [102]. The nude mice have adopted their name from their phenotype; a side-effect of not having a thymus is that they do not have body hair. Based on published literature on the effect of immune system on radioactivity, including alpha therapy (see background, section 3.3), we expect that the immune system will have some contribution to the efficacy of the TTC; as such this is a limitation to using this model. Another limitation is the exploration of the toxicity from the TTCs, as the mice are not suitable models for accurate assessment of toxicity. Nevertheless, the nude mice are considered well suited for growing human xenograft models for standard efficacy evaluation and biodistribution [102]. Further safety assessment has to be further explored in higher models, such as cynomologus monkey.

Procedure: Animal experiments were conducted at the animal research facilities at the Department of Comparative Medicine, Oslo University Hospital, at the animal research facilities at

Bayer AG (Wuppertal, Germany) or at the Laboratory of Pharmatest Services Ltd (Turku, Finland). All experimental protocols were approved by the National Animal Research Authority and the experiments were conducted according to the regulations of the Federation of European Laboratory Animal Science Association (FELASA) and Directive 2010/63/EU of European Parliament.

Anti-tumor Efficacy

Cancer cells were inoculated subcutaneously into the flank of the mice. The TTCs were administered via intravenous (i.v.) injection. The selection of the administered radioactivity range was based on historical data [19, 20]. The activity range of 100-500 kBq/kg bw has previously been demonstrated to be well tolerated and suitable for evaluating specific efficacy and dose-response of the TTCs. PLEASE NOTE: throughout this thesis when referring to a dose in units of kBq/kg this relates to the injected radioactivity at t=0 and not to the total absorbed dose (Gy).

ATRi BAY 1895344 was dosed *per os* (p.o.) and PARPi olaparib dosed intraperitoneal (i.p.). To allow sufficient uptake of the TTC in the tumor and decay of thorium-227 (t 1/2: 18.7 d) to occur, the dosing of the inhibitor was started one week after initiating the TTC dosing. Based on the available biodistribution data, this should allow for sufficient time for uptake of the TTC to occur and it will also minimize the non-specific exposure as the level of circulating TTCs has already decreased.

Tumor growth was measured every second or third day by using a caliper. Body weight was measured every second or third day and animals were sacrificed by cervical dislocation upon reaching the humane endpoint (tumor volume ≥ 1.500 mm^3; body weight loss ≥ 15%). In all studies, animals received an intraperitoneal (i.p.) injection of an unrelated murine IgG2a antibody (200 µg/animal; UPC10; Sigma) 24 hours prior to TTC treatment to block unspecific spleen uptake of the TTC or isotype control [103].

Biodistribution

As specific tumor uptake of TTC and low uptake in normal tissue is essential for the efficacy and safety of the drug, the biodistribution for FGFR2-TTC and HER2-TTC was evaluated. For the MSLN study, data demonstrating specific uptake in the tumor was already available. Factors that influence the biodistribution of antibodies includes expression of the antigen in tumor, antigen shedding and normal tissue expression [104]. Furthermore, tumors are characterized by leaky vessels because of the rapid and uncontrolled vascularization that occur during tumorigenesis. In addition, this characteristic vascularization typically keeps the high-molecular-weight molecules in the tumor for a longer time, a phenomenon called enhanced permeability and retention (EPR) effect [105]. The EPR effect is therefore a contributor to the uptake and retention of the TTCs in the tumor.

Procedure: Organs and tumors were harvested after injection of TTC and radiolabeled isotype control. The biodistribution was evaluated using a high purity germanium detector (Ortec) and detection of thorium-227 was based on known gamma emission energies following release of the alpha particle (Table 6) To identify thorium-227, the GammaVision software and Npp32 analysis engine (Reg. Guide 4.16 detection limit method) were used. Thorium-227 counts were corrected to the time of sacrifice and expressed as percentage (%) of injected dose of ^{227}Th per gram (% ID/g).

Table 6 Gamma Peaks used for Identification and Quantification of thorium-227

Energy (keV)	Yield (%)
235.96	12.90
256.23	7.00
329.85	2.90
286.09	1.74
304.50	1.15
334.37	1.14
299.98	2.21

Calculation of *in vivo* combination effect

For evaluation of combination effect in animal studies the Bliss model was used [106]. Bliss model: C=A+B-A*B; wherein C is the expected T/C of the combination of drug A and drug B if they act additive, A is T/C of drug A, B is T/C of drug B). More than 10% over the expected additive effect is assumed to indicate synergism of the two drugs, less than 10% of the expected additive effect is assumed to indicate antagonism.

Immunohistochemistry

HER2 was stained using SP3 rabbit monoclonal antibody (Spring Biosciences, Pleasanton, CA, USA) and visualized by 3,3'-Diaminobenzidine (DAB). The status (from 0 to +3) was analyzed using ImmunoMembrane web application. The H-score was calculated for the tumor tissue by adding the multiplication of staining intensities in four gradations with each percentage of positive cells yielding a score between 0 and 300 points.

MSLN study: At the study endpoint, the tumors treated with MSLN-TTC (500 kBq/kg) and vehicle groups were stained for γH2A.X using rabbit anti H2A.X antibody (Cat# MABE205 Millipore) with BrightVision rabbit/HRP (Immunologic, DPVR110HRP) followed by visualization with DAB.

6 Summary of Results

6.1 Paper I: Synergistic Effect of a Mesothelin Targeted Thorium-227 Conjugate in Combination with DNA Damage Response Inhibitors in Ovarian Cancer Xenograft Models

This study evaluated the thorium-227 labeled anti-MSLN antibody conjugate and explored efficacy both as monotherapy and in combination with different DDR inhibitors in MSLN-positive cell lines and xenografts in mice.

Initially, synergistic effects of MSLN-TTC and DDR inhibitors were explored in viability assays. The MSLN-TTC was shown to synergize with all DDR inhibitors tested (ATMi, ATRi, DNA-PKi and PARPi) with a more pronounced effect observed for ATRi and PARPi. Mechanistic studies evaluating the ATRi combination on the ovarian OVCAR-3 cell line revealed a significantly higher proportion of cells continuing through the cell cycle into G1/S phase than for the MSLN-TTC monotherapy ($p < 0.0001$). The reduced level of cell cycle arrest for the ATRi combination can be explained by the blockage of the ATR kinase at the G2 cell cycle checkpoint [107]. It also appeared that this combination resulted in a higher level of DSBs as evidenced by γ-H2A.X staining. Furthermore, the potency of the combination was reflected in an increase in apoptosis and reduction in cell viability. In contrast, the PARPi combination appeared to increase cell cycle arrest and γ-H2A.X staining was less pronounced, as was induction of apoptosis markers and cell viability. The cell cycle data therefore appear to reflect key mechanistic differences between ATR, involved in cell cycle arrest and DNA DSB repair and PARP, involved in single strand repair. Interestingly, further investigation of the ATR combination revealed that treatment with the combination induced a reduction in phosphorylated-Chk1 (p-Chk1) as compared to monotherapy with TTCs. As p-Chk1 is the activated version of downstream target of the ATR kinase (see extended data in appendix 1) this is further supporting that the ATRi is in fact inhibiting signaling from the ATR kinase. In

addition, studies revealed that the increased level of DSBs was specific to treatment with MSLN-TTC, demonstrated by comparison with a radiolabeled isotype control (see appendix 2), reflecting the role of the targeting effect of the TTC in the combined treatment as well.

Based on the strong *in vitro* synergy in the ovarian cancer cell line OVCAR-3, this model was used further for *in vivo* evaluation of the combinations of MSLN-TTC with the PARPi and the ATRi. First, a dose response study was performed in OVCAR-3 tumor bearing mice treated with a single dose of 100, 250 or 500 kBq/kg of MSLN-TTC. Significant inhibition of tumor growth was measured at 250 and 500 kBq/kg, while 100 kBq/kg gave no measurable effect on growth inhibition compared to vehicle control. Non-significant efficacy was observed for the isotype control at 250 kBq/kg, which is likely to arise from non-target mediated EPR effect [105]. IHC analysis of γH2A.X indicated higher levels of DSBs in the 500 kBq/kg group compared to vehicle controls further supporting the validity of testing the DDR inhibitor combination in this model at lower doses.

When PARPi was combined with MSLN-TTC at a single dose of 100 kBq/kg, statistical significance was achieved when compared to the vehicle control ($P<0.001$). However, the PARPi combination was not significantly different to the 100 kBq/kg monotherapy treatment. This lack of *in vivo* synergy may serve to highlight that inhibition of SSB repair, mediated by PARP, has a less pronounced effect than targeting DSB repair and cell cycle checkpoint, mediated by ATR, in the response to alpha-radiation induced DNA damage. In contrast, MSLN-TTC at a single dose of 100 kBq/kg combined with ATRi (40 mg/kg), resulted in a more pronounced tumor growth inhibition in comparison to the combination with PARPi. The combination induced significant ($p<0.001$) tumor growth inhibition, the level of this effect being equivalent to the single dose of 250 kBq/kg of MSLN-TTC, and was determined to be strongly synergistic by the Bliss additivity model. This is in alignment with the observations from the *in vitro* studies and further supports the hypothesis that blockage of the DNA double strand break repair machinery results in stronger therapeutic efficacy.

A second human ovarian cancer xenograft model using the OVCAR-8 cell line was selected for further evaluation of the ATRi combination. This model had a lower level of receptors and a more rapid growth rate. The dosing regimen was therefore changed to 3 x 200 kBq/kg administered as monotherapy or in combination with ATRi (40 mg/kg 2QD, 2 days on/ 5 days off). Each single agent (MSLN-TTC or ATRi) induced a significant tumor growth inhibition ($p<0.0001$) compared to vehicle. However, the combination resulted in a significant increase of tumor growth inhibition compared to both monotherapies ($p<0.001$), demonstrating the synergistic activity. All doses were well tolerated as evidenced by no critical body weight loss. Hematological analysis, measuring white blood cells and platelets, showed comparable values after MSLN-TTC monotherapy and the combination with ATRi, indicating that there was no increased toxicity from the combination treatment.

6.2 Paper II: Preclinical Combination Studies of an FGFR2 Targeted Thorium Conjugate and an ATR Inhibitor BAY 1895344

This study evaluated the thorium-227 labeled anti-FGFR2 antibody conjugate and explored efficacy both as monotherapy and in combination with ATR inhibitor BAY 1895344 in FGFR2-positive tumor xenograft models in mice.

The fully humanized monoclonal antibody BAY 1179470 (FGFR2-Ab) binds specifically to FGFR2 with a K_D of 75 nM resulting in efficient receptor-mediated endocytosis of the antibody [32]. Furthermore, the antibody is cross-reactive with murine FGFR2 (K_D of 72 nM) allowing an assessment of the normal tissue distribution in mice. The bioanalytical characterization of the FGFR2-TTC demonstrated that the binding characteristics of the antibody were not impaired by the manufacturing process and the drug product formulation was stable over 48 hours as evidenced by radio-SEC chromatography.

In the panel of FGFR2 expressing human cell lines MFM-223, KATO III and SUM52-PE, a significant reduction of cell viability was demonstrated for the combination compared to monotherapy at all doses tested. Mechanistic analyses revealed that treatment with FGFR2-TTC alone led to the induction of G2/M cell cycle arrest suggesting activation of DNA damage response pathways. However when combined with ATRi, the number of cells in G2/M phase decreased compared to FGFR2-TTC monotherapy indicative of the abrogation of cell cycle arrest. In addition, increased numbers of DNA DSBs were detected by analysis of γH2A.X in all cell lines treated with FGFR2-TTC in what appeared to be a dose-dependent manner. This effect was further accentuated in the combination groups as evidenced by both decreased cell viability and increased γH2A.X staining indicating a potential synergistic effect of the combination.

Next, biodistribution studies were performed to discriminate specific from non-specific uptake in the tumor, the latter arising from the EPR effect. The overall organ distribution was similar with the exception of the tumor uptake with >40 % ID/g for the FGFR2-TTC compared to <10 % ID/g tumor for the isotype control at day 7 indicating specific accumulation. The biodistribution demonstrated relatively low levels of uptake in all organs and was not significantly different to the isotype control, indicating that target binding in normal tissues may not be an issue. FGFR2-TTC efficacy was then assessed as a monotherapy in the NCI-H716, SNU-16 and MFM-223 tumor models. Administration of a single dose of 500 kBq/kg resulted in statistical significant inhibition of tumor growth in all three models whereas the lower radioactive doses of 100 and 250 kBq/kg had no effect.

The *in vivo* efficacy of the combination was then evaluated in the MFM-223 xenograft model utilizing non-efficacious monotherapy doses of both FGFR2-TTC and ATRi. A dose of 100 kBq/kg was combined with ATRi BAY 1895344 p.o. dosed at 40 mg/kg twice daily for three days on and four days off over a period of four weeks. Furthermore, as accumulation of the FGFR2-TTC reached a maximum in the tumor at 168 hours, the dosing of BAY 1895344 was initiated one week post FGFR2-TTC administration to allow for accumulation of DNA damage. Statistically significant tumor growth inhibition was indeed observed only for the combination ($P < 0.01$) and was determined to be synergistic based on the Bliss model [106]. All treatments were well tolerated as evidenced by no loss in body weight throughout the study.

6.3 Paper III: Synergistic Effect of a HER2 Targeted Thorium-227 Conjugate in Combination with olaparib in a BRCA2 Deficient Xenograft Model

In the final study the thorium-227 labeled anti-HER2 antibody conjugate was evaluated together with the PARPi olaparib in a BRCA2 defect model as compared to the BRCA2 functional parental model. Since olaparib is known to induce synthetic lethality in BRCA mutated tumors [75], the BRCA2 deficient cancer cell line (DLD-1 BRCA2 -/-) was selected for this study. As the primary mode of action of the TTC is induction of complex DNA damage we hypothesized that 1) the BRCA2 knockout would sensitize to TTC treatment and 2) that the combination with PARPi would be synergistic. Identical data sets were also generated in the BRCA2 proficient parental cell line (DLD-1 parental) for comparison.

First, a clear difference was observed *in vitro* with the BRCA2 -/- cell line demonstrating increased sensitivity to HER2-TTC and clear synergistic effect from the combination based on the calculated combination index compared to the parental cell line. The *in vivo* analysis revealed a similar picture. Biodistribution and retention was shown to be specific as evidenced by the high tumor uptake in both models for HER2-TTC (40-60 % ID/g) compared to ca. 5% ID/g for the isotype control at 336 h [108]. Interestingly significant tumor growth inhibition was achieved for the TTC monotherapy at the higher doses of 300 and 600 kBq/kg. In light of the low HER2 expression measured by both FACS and H-Score, this data may support the further investigation of HER2-TTC as a monotherapy in patients who are currently HER2 positive but not deemed suitable for either Herceptin or Kadcyla based on biopsy. Furthermore, several of the current obstacles with drug resistance, such as change in signaling pathways, enhanced efflux pumps or lack of internalization, are not necessarily relevant for the treatment with alpha therapy based on the known mechanism of action.

A strong synergistic effect was observed using the combination of the two non-effective monotherapy doses (120 kBq/kg bw, 50 mg/kg bw daily, 4 weeks) which resulted in a robust tumor growth inhibition. Furthermore, no significant myelosuppression was observed for the combination on the red and white blood cells as well as platelet populations.

7 Discussion

The field of oncology is continuously advancing both in areas of basic research and the development of novel strategies targeted at the Achilles heel of the cancer cell. Although great progress has been made, the three pillars of cancer therapy; surgery, radiation and chemotherapy, still remain the cornerstone of treatment. In addition, even though the new modalities such as immunotherapy and precision drugs have demonstrated great utility there still remains a clear need for new approaches which address the challenges of developing drug- and radio-resistance and provide new options on treatment relapse. As such, cancer remains a leading cause of death worldwide and new innovative therapeutic approaches are still necessary [109].

Although there have been many clinical trials for RIT during recent years there are only two therapies that have been approved by the FDA, both of them targeting hematological tumors. The lack of success with solid tumors can be partially explained by the fact that they appear to be more radioresistant as compared to hematological cancers [17]. DNA damage repair has been demonstrated to affect the outcome of treatment with radiotherapy and multiple studies with low LET radiation combined with DDR inhibitors have shown to be advantageous as it has potential to sensitize the cancer cells to therapy. Furthermore, the general use of combination therapy with synergistic drug modalities may have several benefits such as enhanced efficacy and capacity to overcome drug resistance, as well as reduced side effects experienced by the patient [100]. As such, the goal of the work presented was to provide initial evidence that the combination therapy with

TTCs and DDR inhibitors increases the therapeutic window by sensitizing the tumors through induction of DSBs and inhibition of subsequent repair.

In the studies presented, the effect of DDR inhibitors in combination with TTCs were investigated utilizing three antibodies targeted to three different cancer specific antigens. The findings demonstrate that it was possible to achieve synergistic effect in combination with DDR inhibitors and that this effect was linked to increased level of DSBs. Overall, the ATRi combination showed most potent induction of synergy both *in vitro* and *in vivo*, with clear synergistic effect in two ovarian cancer xenograft models and a breast cancer xenograft model. While the PARPi olaparib, demonstrated clear synergistic effect only in the BRCA2 knockout model and additive effect in the parental BRCA2 functional model as well as in ovarian cancer model carrying no known relevant mutations for olaparib treatment.

A plausible explanation for the more potent induction of synergy with the ATR combination may be the potency of alpha emitters in inducing DSBs combined with the central role of the ATR kinase in DSB repair, in contrast to PARP involved in SSB repair. In addition, abrogation of the G2 cell cycle checkpoint followed with accumulation of DNA damage caused by the TTC could also be a possible explanation for the observed synergy. The selective blocking of the G2 checkpoint together with ionizing radiation has previously been reported to trigger mitotic catastrophe, as the cell continues to divide without repairing the damage [90, 107]. Since cancers frequently have defects in P53, which affect their ability to initiate cell cycle arrest in G1 and S phase of the cell cycle, they are more reliant on the arrest in the G2 phase. As seen after treatment with TTC as a single agent, the cells accumulate with 4N DNA content, indicating arrest in G2 or M phase. Due to the dependency of the G2/M checkpoint, ATRi has been reported to induce synthetic lethality in tumors with defects in G1 cell cycle checkpoint, including mutations in ATM and TP53 [107]. This dependency on G2 arrest may also be a possible explanation for the high potency of ATRi to induce synergistic effect in our

studies. All the three xenograft models tested for the ATRi combination, OVCAR-3 ($TP53^{mut}$), OVCAR-8 (ATM^{mut}/ $TP53^{mut}$) and MFM-223 ($TP53^{mut}$), carry relevant mutations in this context [110], which may have contributed to the potency of the ATRi in inducing synergistic effect.

Current treatment modalities, including radio- and chemotherapy are generally highly efficient, however generation of robust responses to the treatment are limited due to normal tissue toxicity. The use of synergistic drug modalities may offer the opportunity to increase the therapeutic window. The dose-limiting organ when using RIT is the bone marrow, due to the systemic administration and the intrinsic radiosensitivity of the blood cells. Nevertheless, the toxicity profile in patients treated with alpha emitters in RIT applications, such as bismuth-213 and actinium-225, have previously been shown to be acceptable [18]. Radium-223, clinically approved for the treatment of castration resistant prostate cancer, has a very benign toxicity profile as evidenced by the positive outcomes from the many patients treated with the drug in addition to the data from the ALSYMPCA clinical trial [24]. Xofigo® (radium-223 dichloride) was reported to have no dose-limiting hematological toxicity in the dose range 50-250 kBq/kg [111, 112]. Taken together this holds promise for the tolerability of targeted alpha therapies including TTCs which are currently being explored in several clinical phase I studies. In the MSLN study described herein, both the monotherapy and combination therapy were well tolerated as evidenced by no critical body weight loss. Furthermore, the hematological analysis showed comparable values of MSLN-TTC monotreatment and the combination with ATRi, indicating that there was no increased toxicity from the combination treatment. Also, the HER2 studies demonstrated tolerability to treatment, based on body weight measurement and hematological analysis after monotherapy treatment with olaparib and also for the combination with HER2-TTC.

Moreover, the selectivity for the cancer cell compared to normal tissue is important for development of a successful drug as this may also increase the therapeutic window. As such, the

specific targeting of the TTC as well as the selective synergy demonstrated for the BRCA defect model reflects the potential for a cancer specific treatment strategy. If this is translatable to specific DDR mutations, it may be possible in the future to select patients based on precision medicine, selecting exactly those patients who will benefit from the combination based on their mutational status of common DDR genes.

8 Main Conclusions and Future work

The preclinical evaluation of the anti-tumor activity of TTCs and DDR inhibitors demonstrated synergistic effects from the combination treatment, showing an enhanced effect at lower doses of both treatment modalities. Together, the three studies are indicating: 1) a clear synergistic effect of combination of ATRi with TTCs *in vitro* and *in vivo* in breast and ovarian cancer xenografts and 2) A clear synergistic effect of TTC in combination with PARPi in a BRCA2 deficient colorectal xenograft model which appear to be highly dependent on the mutational status/ synthetic lethality.

Taken together, this treatment strategy may have potential to improve the outcome after TTC treatment and reduce side effects experienced by the patients. As such, our findings support the further exploration of TTCs in combination with DDR inhibitors for treatment of different cancer indications.

The following topics are relevant to explore in future studies:

Synthetic lethality approaches

As already exemplified with PARPi/TTC and the BRCA2 knockout model, genetic defects may increase the specificity and efficacy of the treatment. As such, a broader assessment of the relevance of targeting specific mutations in relation to synergy should be performed in pre-clinical studies.

For the PARPi/TTC study clinical relevant cancer indications should be explored further. The DLD-1 cell line was used as a model for investigating the influence of the BRCA2 mutation in the context of TTC/PARPi combination effect. However, as BRCA2 deficient/HER2 positive colorectal cancer do not represent a large patient group, further examination of BRCA2 defects across all cancer types should be performed. Thus, continued work on this combination therapy should include cancer indications known to carry both upregulation of a relevant TTC target and BRCA mutations. As such, breast and ovarian cancer may be more suitable indications for this combination treatment [62, 74]. Furthermore, several other HR defects, including defects in ATM and RAD51 [114], have also demonstrated to sensitize cells to PARP treatment and could therefore also be of interest to explore in context of synthetic lethality in combination with TTCs.

As discussed for ATRi, defects in ATM or the downstream TP53 have demonstrated sensitization to ATRi treatment. Defects in this pathway pre-dispose to development of cancer and have been seen in up to 70 % of tumors [89], thus mutations in this pathway may serve as relevant biomarker for combination therapy of TTCs with ATRi. Although the models included in the MSLN-TTC study contained relevant mutations, i.e. ATM and TP53, the influence of these defects needs to be investigated further in isogenic models, comparing the ATRi/TTC combination therapy in a parental and knockout model.

Relevance of dosing levels and schedule

One of the challenges with combination therapy is to find an optimal dosing schedule. As such, it is relevant to explore how different dose schedules may influence the outcome of the treatment with respect to the combination effect as well as the level of synergy. This includes studies investigating different radioactivity levels and DDR doses, and the dose sequence/timing of the two drug modalities.

Immune mediated effects

Since alpha therapy has already demonstrated to trigger activation of the immune system including abscopal effects, it is relevant to explore the efficacy of TTC treatment in immune competent animal models, such as BALB/c or C57BL/6 mice. Furthermore, preclinical studies with another ATRi (AZD6738), which is in clinical trials in combination with radiotherapy (NCT02223923), have demonstrated enhanced immune activation in combination with low LET radiation (X-ray) [115]. These studies indicate that a TTC/ATRi combination could induce an immune activation, potentiating the efficacy further and would therefore be of interest to explore in immune competent models.

Increase the scope of combination therapies with TTCs

Based on the limited investigation of TTC/DDR inhibitor combinations, ATMi and DNA-PKi should be investigated further on different cancer cell lines. Several studies support the relevance of both DNA-PK and ATM in sensitization to radiation therapy, including combination therapy with another alpha-emitter, bismuth-213 [67]. Furthermore, it is also of interest to explore combination therapies that are not directly linked to DDR pathways. For example checkpoint inhibitors may have potential to enhance the effect as alpha emitters have already demonstrated activation of immune response.

Explore DDR genes as potential biomarkers

Several cancer therapies are now being approved in cancer indications carrying DDR defects, such as olaparib approved for BRCA mutated ovarian and breast cancer and nivolumab approved for mismatch repair deficient (dMMR) or microsatellite instability-high (MSI-H) colorectal cancer. In 2017 another of the checkpoint inhibitors, pembrolizumab, was FDA approved for treatment of solid tumors with MSI-H or dMMR, thus being the first drug approved on the basis of genetic defects without link to cancer indication. Expanding on the data presented in the thesis, patients with defects in DDR may be particularly sensitive to TTC treatment. As such, in future clinical studies it could be of interest to investigate the relation between mutational status of DDR genes, such as BRCA1/2, and patients that respond well to TTC treatment.

Translating treatment to clinical practice

The efficacy, tolerability and commercialization of the drug products are important factors for enabling the translation of treatment to clinical practice. Unlike the alpha-emitter actinium-225, which decays to bismuth-213, a kidney-avid radionuclide [116], radium-223 has poor affinity for biological systems (protein binding and organ retention) and is excreted rapidly through the small intestine [117, 118]. On the other hand, a proportion of the radium-223 can be incorporated into bone. The ALSYMPCA clinical trial clearly demonstrated the acceptable tolerability of bone deposition [24] which is also central in the context of the TTCs, since alpha-particle decay of thorium-227 results in the generation of non-chelator bound radium-223. The on-going clinical studies for TTCs will further address the tolerability of the treatment, including the front-runner clinical phase I program targeting CD22 (NCT02581878), which is currently in dose escalation phase in patients with relapsed or refractory CD22-positive non-Hodgkin lymphoma. This study will answer many questions around the general tolerability of TTCs in humans. In addition phase I studies of the DDR inhibitors will also give an indication as to dosing levels suitable for planning combination studies.

Since bone marrow hematopoietic stem cells are highly sensitive to radiation, myelosuppression is considered to be dose-limiting as has been demonstrated for many RIT applications with beta and alpha emitters. It remains to be seen if an acceptable therapeutic window can be achieved with TTCs in combination with DDR inhibitors.

The commercialization of radiopharmaceuticals has historically been challenged with high costs, limited supply and short half-life giving logistical limitations for the production. In fact, one of the RITs that have been approved for treatment, Bexxar®, was taken out of production in 2013 due to non-competitive pricing and complexity of supply chain. Building on the already established supply chain and experience with distribution of the alpha emitter radium-223 (Xofigo®) has enabled the efficient delivery of TTCs to patients, as shown by the ongoing clinical phase I studies with CD22-TTC, MSLN-TTC and PSMA-TTC. The drug can be a produced via a central radiopharmacy which finalizes the production of the TTCs and then distributes to various medical centers in the region within 24-48 hours, which is an acceptable time frame considering the half-life of thorium-227 and the stability of the product. Furthermore, using actinium-227, the same starting material used in the manufacture of radium-223, we also have a steady and cost-efficient supply of thorium-227 which is the first daughter of actinium-227.

In conclusion, TTCs show great promise to be a new treatment modality in the fight against cancers with unmet medical need.

9 References

1. Smyth, M.J., *Multiple approaches to immunotherapy - the new pillar of cancer treatment.* Immunol Cell Biol, 2017. 95(4): p. 323-324.

2. McCarthy, E.F., *The toxins of William B. Coley and the treatment of bone and soft-tissue sarcomas.* Iowa Orthop J, 2006. 26: p. 154-8.

3. Lutterotti, A. and R. Martin, *Getting specific: monoclonal antibodies in multiple sclerosis.* Lancet Neurol, 2008. 7(6): p. 538-47.

4. Hansel, T.T., et al., *The safety and side effects of monoclonal antibodies.* Nat Rev Drug Discov, 2010. 9(4): p. 325-38.

5. Kohler, G. and C. Milstein, *Continuous cultures of fused cells secreting antibody of predefined specificity.* Nature, 1975. 256(5517): p. 495-7.

6. *Monoclonal Antibodies Approved by the EMA and FDA for Therapeutic Use (status 2017)*. Available from: http://www.actip.org/products/monoclonal-antibodies-approved-by-the-ema-and-fda-for-therapeutic-use/.

7. Baxevanis, C.N., S.A. Perez, and M. Papamichail, *Cancer immunotherapy.* Crit Rev Clin Lab Sci, 2009. 46(4): p. 167-89.

8. *Radiation Therapy for Cancer*. Available from: https://www.cancer.gov/about-cancer/treatment/types/radiation-therapy/radiation-fact-sheet.

9. Martins, C.D., G. Kramer-Marek, and W.J.G. Oyen, *Radioimmunotherapy for delivery of cytotoxic radioisotopes: current status and challenges.* Expert Opin Drug Deliv, 2017.

10. Gudkov, S.V., et al., *Targeted Radionuclide Therapy of Human Tumors.* Int J Mol Sci, 2016. 17(1).

11. Goldsmith, S.J., *Radioimmunotherapy of lymphoma: Bexxar and Zevalin.* Semin Nucl Med, 2010. 40(2): p. 122-35.

12. Barber, T.W., et al., *Clinical outcomes of (177)Lu-PSMA radioligand therapy in taxane chemotherapy pretreated and taxane chemotherapy naive patients with metastatic castration resistant prostate cancer.* J Nucl Med, 2019.

13. Sgouros, G., et al., *MIRD Pamphlet No. 22 (abridged): radiobiology and dosimetry of alpha-particle emitters for targeted radionuclide therapy.* J Nucl Med, 2010. 51(2): p. 311-28.

14. Carter, R.J., et al., *Complex DNA Damage Induced by High Linear Energy Transfer Alpha-Particles and Protons Triggers a Specific Cellular DNA Damage Response.* Int J Radiat Oncol Biol Phys, 2018. 100(3): p. 776-784.

15. Sage, E. and N. Shikazono, *Radiation-induced clustered DNA lesions: Repair and mutagenesis.* Free Radic Biol Med, 2017. 107: p. 125-135.

16. Frankenberg-Schwager, M., D. Frankenberg, and R. Harbich, *Repair of DNA double-strand breaks as a determinant of RBE of alpha particles.* Br J Cancer Suppl, 1984. 6: p. 169-73.

17. Pouget, J.P., et al., *Clinical radioimmunotherapy--the role of radiobiology.* Nat Rev Clin Oncol, 2011. 8(12): p. 720-34.

18. Targeted Alpha Therapy Working, G., *Targeted alpha therapy, an emerging class of cancer agents: A review.* JAMA Oncology, 2018.

19. Hagemann, U.B., et al., *In Vitro and In Vivo Efficacy of a Novel CD33-Targeted Thorium-227 Conjugate for the Treatment of Acute Myeloid Leukemia.* Mol Cancer Ther, 2016. 15(10): p. 2422-2431.

20. Hagemann, U.B., et al., *Targeted alpha therapy using a novel CD70 targeted thorium-227 conjugate in in vitro and in vivo models of renal cell carcinoma.* Oncotarget, 2017.

21. Karlsson, J., et al., *HER2-targeted thorium-227 conjugate (HER2-TTC): Efficacy in preclinical models of trastuzumab and T-DM1 resistance.* AACR Annual Meeting 2017; April 1-5, 2017; Washington, DC, 2017. DOI: 10.1158/1538-7445.AM2017-5859 Published July 2017.

22. Hammer, S., et al., *Preclinical pharmacology of the PSMA-targeted thorium-227 conjugate PSMA-TTC: a novel targeted alpha therapeutic for the treatment of prostate cancer.* AACR Annual Meeting 2017; April 1-5, 2017; Washington, DC, 2017. DOI: 10.1158/1538-7445.AM2017-5200 Published July 2017.

23. Karlsson, J., et al., *HER2-targeted thorium-227 conjugate (HER2-TTC): Efficacy in a HER2 positive orthotopic bone model.* AACR Annual Meeting 2017; April 1-5, 2017; Washington, DC, 2017. DOI: 10.1158/1538-7445.AM2017-5857 Published July 2017.

24. Parker, C., et al., *Alpha emitter radium-223 and survival in metastatic prostate cancer.* N Engl J Med, 2013. 369(3): p. 213-23.

25. Ramdahl, T., et al., *An efficient chelator for complexation of thorium-227.* Bioorg Med Chem Lett, 2016. 26(17): p. 4318-21.

26. Deblonde, G.J., et al., *Solution Thermodynamics and Kinetics of Metal Complexation with a Hydroxypyridinone Chelator Designed for Thorium-227 Targeted Alpha Therapy.* Inorg Chem, 2018.

27. Chang, J., et al., *Prognostic value of FGFR gene amplification in patients with different types of cancer: a systematic review and meta-analysis.* PLoS One, 2014. 9(8): p. e105524.

28. Roskoski, R., Jr., *The ErbB/HER family of protein-tyrosine kinases and cancer.* Pharmacol Res, 2014. 79: p. 34-74.

29. Tang, Z., M. Qian, and M. Ho, *The role of mesothelin in tumor progression and targeted therapy.* Anticancer Agents Med Chem, 2013. 13(2): p. 276-80.

30. Rump, A., et al., *Binding of ovarian cancer antigen CA125/MUC16 to mesothelin mediates cell adhesion.* J Biol Chem, 2004. 279(10): p. 9190-8.

31. Golfier, S., et al., *Anetumab ravtansine: a novel mesothelin-targeting antibody-drug conjugate cures tumors with heterogeneous target expression favored by bystander effect.* Mol Cancer Ther, 2014. 13(6): p. 1537-48.

32. Sommer, A., et al., *Preclinical Efficacy of the Auristatin-Based Antibody-Drug Conjugate BAY 1187982 for the Treatment of FGFR2-Positive Solid Tumors.* Cancer Res, 2016. 76(21): p. 6331-6339.

33. Parakh, S., et al., *Evolution of anti-HER2 therapies for cancer treatment.* Cancer Treat Rev, 2017. 59: p. 1-21.

34. Rexer, B.N. and C.L. Arteaga, *Intrinsic and acquired resistance to HER2-targeted therapies in HER2 gene-amplified breast cancer: mechanisms and clinical implications.* Crit Rev Oncog, 2012. 17(1): p. 1-16.

35. Barok, M., H. Joensuu, and J. Isola, *Trastuzumab emtansine: mechanisms of action and drug resistance.* Breast Cancer Res, 2014. 16(2): p. 209.

36. Turner, N. and R. Grose, *Fibroblast growth factor signalling: from development to cancer.* Nat Rev Cancer, 2010. 10(2): p. 116-29.

37. Bharadwaj, U., et al., *Mesothelin overexpression promotes autocrine IL-6/sIL-6R trans-signaling to stimulate pancreatic cancer cell proliferation.* Carcinogenesis, 2011. 32(7): p. 1013-24.

38. Chan, K.M., et al., *MT1-MMP inactivates ADAM9 to regulate FGFR2 signaling and calvarial osteogenesis.* Dev Cell, 2012. 22(6): p. 1176-90.

39. Ghedini, G.C., et al., *Shed HER2 extracellular domain in HER2-mediated tumor growth and in trastuzumab susceptibility.* J Cell Physiol, 2010. 225(1): p. 256-65.

40. Pastan, I. and Y. Zhang, *Modulating mesothelin shedding to improve therapy.* Oncotarget, 2012. 3(2): p. 114-5.

41. Klapper, L.N., et al., *Tumor-inhibitory antibodies to HER-2/ErbB-2 may act by recruiting c-Cbl and enhancing ubiquitination of HER-2.* Cancer Res, 2000. 60(13): p. 3384-8.

42. Lorat, Y., et al., *Clustered double-strand breaks in heterochromatin perturb DNA repair after high linear energy transfer irradiation.* Radiother Oncol, 2016. 121(1): p. 154-161.

43. Lindahl, T. and D.E. Barnes, *Repair of endogenous DNA damage.* Cold Spring Harb Symp Quant Biol, 2000. 65: p. 127-33.

44. Thompson, L.H., *Recognition, signaling, and repair of DNA double-strand breaks produced by ionizing radiation in mammalian cells: the molecular choreography.* Mutat Res, 2012. 751(2): p. 158-246.

45. Konecny, G.E. and R.S. Kristeleit, *PARP inhibitors for BRCA1/2-mutated and sporadic ovarian cancer: current practice and future directions.* Br J Cancer, 2016. 115(10): p. 1157-1173.

46. Krejci, L., et al., *Homologous recombination and its regulation.* Nucleic Acids Res, 2012. 40(13): p. 5795-818.

47. O'Connor, M.J., *Targeting the DNA Damage Response in Cancer.* Mol Cell, 2015. 60(4): p. 547-60.

48. Bennett, C.B., et al., *Lethality induced by a single site-specific double-strand break in a dispensable yeast plasmid.* Proc Natl Acad Sci U S A, 1993. 90(12): p. 5613-7.

49. Tamulevicius, P., M. Wang, and G. Iliakis, *Homology-directed repair is required for the development of radioresistance during S phase: interplay between double-strand break repair and checkpoint response.* Radiat Res, 2007. 167(1): p. 1-11.

50. Hanahan, D. and R.A. Weinberg, *Hallmarks of cancer: the next generation.* Cell, 2011. 144(5): p. 646-74.

51. Vousden, K.H. and X. Lu, *Live or let die: the cell's response to p53.* Nat Rev Cancer, 2002. 2(8): p. 594-604.

52. Lowe, S.W., et al., *p53 is required for radiation-induced apoptosis in mouse thymocytes.* Nature, 1993. 362(6423): p. 847-9.

53. Baidoo, K.E., K. Yong, and M.W. Brechbiel, *Molecular pathways: targeted alpha-particle radiation therapy.* Clin Cancer Res, 2013. 19(3): p. 530-7.

54. Gorin, J.B., et al., *Alpha Particles Induce Autophagy in Multiple Myeloma Cells.* Front Med (Lausanne), 2015. 2: p. 74.

55. Mukherjee, S. and A. Chakraborty, *Radiation Induced Bystander Phenomenon: Insight and Implications in Radiotherapy.* Int J Radiat Biol, 2018: p. 1-48.

56. Siva, S., et al., *Abscopal effects of radiation therapy: a clinical review for the radiobiologist.* Cancer Lett, 2015. 356(1): p. 82-90.

57. Mole, R.H., *Whole body irradiation; radiobiology or medicine?* Br J Radiol, 1953. 26(305): p. 234-41.

58. Demaria, S., et al., *Ionizing radiation inhibition of distant untreated tumors (abscopal effect) is immune mediated.* Int J Radiat Oncol Biol Phys, 2004. 58(3): p. 862-70.

59. Malamas, A.S., et al., *Sublethal exposure to alpha radiation (223Ra dichloride) enhances various carcinomas' sensitivity to lysis by antigen-specific cytotoxic T lymphocytes through calreticulin-mediated immunogenic modulation.* Oncotarget, 2016. 7(52): p. 86937-86947.

60. Harrington, K., P. Jankowska, and M. Hingorani, *Molecular biology for the radiation oncologist: the 5Rs of radiobiology meet the hallmarks of cancer.* Clin Oncol (R Coll Radiol), 2007. 19(8): p. 561-71.

61. Weber, A.M. and A.J. Ryan, *ATM and ATR as therapeutic targets in cancer.* Pharmacol Ther, 2015. 149: p. 124-38.

62. Alsop, K., et al., *BRCA mutation frequency and patterns of treatment response in BRCA mutation-positive women with ovarian cancer: a report from the Australian Ovarian Cancer Study Group.* J Clin Oncol, 2012. 30(21): p. 2654-63.

63. Reilly, N.M., et al., *Exploiting DNA repair defects in colorectal cancer.* Mol Oncol, 2019.

64. Bao, S., et al., *Glioma stem cells promote radioresistance by preferential activation of the DNA damage response.* Nature, 2006. 444(7120): p. 756-60.

65. Lucchesi, J.C., *Synthetic lethality and semi-lethality among functionally related mutants of Drosophila melanfgaster.* Genetics, 1968. 59(1): p. 37-44.

66. Oliveira, N.G., et al., *Wortmannin enhances the induction of micronuclei by low and high LET radiation.* Mutagenesis, 2003. 18(1): p. 37-44.

67. Song, H., et al., *Targeting aberrant DNA double-strand break repair in triple-negative breast cancer with alpha-particle emitter radiolabeled anti-EGFR antibody.* Mol Cancer Ther, 2013. 12(10): p. 2043-54.

68. Ame, J.C., C. Spenlehauer, and G. de Murcia, *The PARP superfamily.* Bioessays, 2004. 26(8): p. 882-93.

69. d'Adda di Fagagna, F., et al., *Functions of poly(ADP-ribose) polymerase in controlling telomere length and chromosomal stability.* Nat Genet, 1999. 23(1): p. 76-80.

70. Ame, J.C., et al., *PARP-2, A novel mammalian DNA damage-dependent poly(ADP-ribose) polymerase.* J Biol Chem, 1999. 274(25): p. 17860-8.

71. Kim, M.Y., T. Zhang, and W.L. Kraus, *Poly(ADP-ribosyl)ation by PARP-1: 'PAR-laying' NAD+ into a nuclear signal.* Genes Dev, 2005. 19(17): p. 1951-67.

72. Jacobson, E.L., et al., *Cellular recovery of dividing and confluent C3H10T1/2 cells from N-methyl-N'-nitro-N-nitrosoguanidine in the presence of ADP-ribosylation inhibitors.* Carcinogenesis, 1985. 6(5): p. 715-8.

73. Masutani, M., et al., *Role of poly(ADP-ribose) polymerase in cell-cycle checkpoint mechanisms following gamma-irradiation.* Biochimie, 1995. 77(6): p. 462-5.

74. Farmer, H., et al., *Targeting the DNA repair defect in BRCA mutant cells as a therapeutic strategy.* Nature, 2005. 434(7035): p. 917-21.

75. Benafif, S. and M. Hall, *An update on PARP inhibitors for the treatment of cancer.* Onco Targets Ther, 2015. 8: p. 519-28.

76. Murai, J., et al., *Trapping of PARP1 and PARP2 by Clinical PARP Inhibitors.* Cancer Res, 2012. 72(21): p. 5588-99.

77. Abraham, R.T., *Mammalian target of rapamycin: immunosuppressive drugs uncover a novel pathway of cytokine receptor signaling.* Curr Opin Immunol, 1998. 10(3): p. 330-6.

78. Shiloh, Y. and Y. Ziv, *The ATM protein kinase: regulating the cellular response to genotoxic stress, and more.* Nat Rev Mol Cell Biol, 2013. 14(4): p. 197-210.

79. Falck, J., et al., *The ATM-Chk2-Cdc25A checkpoint pathway guards against radioresistant DNA synthesis.* Nature, 2001. 410(6830): p. 842-7.

80. Cortez, D., et al., *Requirement of ATM-dependent phosphorylation of brca1 in the DNA damage response to double-strand breaks.* Science, 1999. 286(5442): p. 1162-6.

81. Lee, J.H., et al., *53BP1 promotes ATM activity through direct interactions with the MRN complex.* Embo j, 2010. 29(3): p. 574-85.

82. Tang, J., et al., *Acetylation limits 53BP1 association with damaged chromatin to promote homologous recombination.* Nat Struct Mol Biol, 2013. 20(3): p. 317-25.

83. Choi, M., T. Kipps, and R. Kurzrock, *ATM Mutations in Cancer: Therapeutic Implications.* Mol Cancer Ther, 2016. 15(8): p. 1781-91.

84. Savitsky, K., et al., *A single ataxia telangiectasia gene with a product similar to PI-3 kinase.* Science, 1995. 268(5218): p. 1749-53.

85. Saldivar, J.C., D. Cortez, and K.A. Cimprich, *The essential kinase ATR: ensuring faithful duplication of a challenging genome.* Nat Rev Mol Cell Biol, 2017. 18(10): p. 622-636.

86. Fokas, E., et al., *Targeting ATR in DNA damage response and cancer therapeutics.* Cancer Treat Rev, 2014. 40(1): p. 109-17.

87. Shiloh, Y., *ATM and ATR: networking cellular responses to DNA damage.* Curr Opin Genet Dev, 2001. 11(1): p. 71-7.

88. Balmus, G., et al., *Disease severity in a mouse model of ataxia telangiectasia is modulated by the DNA damage checkpoint gene Hus1.* Hum Mol Genet, 2012. 21(15): p. 3408-20.

89. Reaper, P.M., et al., *Selective killing of ATM- or p53-deficient cancer cells through inhibition of ATR.* Nat Chem Biol, 2011. 7(7): p. 428-30.

90. Dillon, M.T., et al., *Radiosensitization by the ATR Inhibitor AZD6738 through Generation of Acentric Micronuclei.* Mol Cancer Ther, 2017. 16(1): p. 25-34.

91. Li, Z., et al., *The XRCC4 gene encodes a novel protein involved in DNA double-strand break repair and V(D)J recombination.* Cell, 1995. 83(7): p. 1079-89.

92. Grawunder, U., et al., *Activity of DNA ligase IV stimulated by complex formation with XRCC4 protein in mammalian cells.* Nature, 1997. 388(6641): p. 492-5.

93. Timme, C.R., et al., *The DNA-PK Inhibitor VX-984 Enhances the Radiosensitivity of Glioblastoma Cells Grown In Vitro and as Orthotopic Xenografts.* Mol Cancer Ther, 2018. 17(6): p. 1207-1216.

94. Bonner, J.A., et al., *Radiotherapy plus cetuximab for locoregionally advanced head and neck cancer: 5-year survival data from a phase 3 randomised trial, and relation between cetuximab-induced rash and survival.* Lancet Oncol, 2010. 11(1): p. 21-8.

95. Mukherjee, B., et al., *EGFRvIII and DNA double-strand break repair: a molecular mechanism for radioresistance in glioblastoma.* Cancer Res, 2009. 69(10): p. 4252-9.

96. Abbas, N., et al., *Experimental alpha-particle radioimmunotherapy of breast cancer using 227Th-labeled p-benzyl-DOTA-trastuzumab.* EJNMMI Res, 2011. 1(1): p. 18.

97. Lindmo, T., et al., *Determination of the immunoreactive fraction of radiolabeled monoclonal antibodies by linear extrapolation to binding at infinite antigen excess.* J Immunol Methods, 1984. 72(1): p. 77-89.

98. Wortmann L, L.U., Lefranc J, Briem H, Koppitz M, Eis K, et al., *2-(Morpholin-4-yl)-1,7-naphthyridines* 2016: Germany

99. Tallarida, R.J., *An overview of drug combination analysis with isobolograms.* J Pharmacol Exp Ther, 2006. 319(1): p. 1-7.

100. Chou, T.C., *Theoretical basis, experimental design, and computerized simulation of synergism and antagonism in drug combination studies.* Pharmacol Rev, 2006. 58(3): p. 621-81.

101. Kuo, L.J. and L.X. Yang, *Gamma-H2AX - a novel biomarker for DNA double-strand breaks.* In Vivo, 2008. 22(3): p. 305-9.

102. Szadvari, I., O. Krizanova, and P. Babula, *Athymic nude mice as an experimental model for cancer treatment.* Physiol Res, 2016. 65(Supplementum 4): p. S441-s453.

103. Reddy, N., et al., *Rapid blood clearance of mouse IgG2a and human IgG1 in many nude and nu/+ mouse strains is due to low IgG2a serum concentrations.* Cancer Immunol Immunother, 1998. 46(1): p. 25-33.

104. Tabrizi, M., G.G. Bornstein, and H. Suria, *Biodistribution mechanisms of therapeutic monoclonal antibodies in health and disease.* Aaps j, 2010. 12(1): p. 33-43.

105. Maeda, H., H. Nakamura, and J. Fang, *The EPR effect for macromolecular drug delivery to solid tumors: Improvement of tumor uptake, lowering of systemic toxicity, and distinct tumor imaging in vivo.* Adv Drug Deliv Rev, 2013. 65(1): p. 71-9.

106. Bliss, C.I., *The toxicity of poisons applied jointly. .* Ann. Appl. Biol., 1939(26): p. 585-615.

107. Dillon, M.T., J.S. Good, and K.J. Harrington, *Selective targeting of the G2/M cell cycle checkpoint to improve the therapeutic index of radiotherapy.* Clin Oncol (R Coll Radiol), 2014. 26(5): p. 257-65.

108. Maeda, H., *Macromolecular therapeutics in cancer treatment: the EPR effect and beyond.* J Control Release, 2012. 164(2): p. 138-44.

109. *Cancer Facts & Figures 2015*, in *American Cancer Society* 2015

110. *COSMIC: somatic cancer genetics at high-resolution*.

111. Nilsson, S., et al., *Bone-targeted radium-223 in symptomatic, hormone-refractory prostate cancer: a randomised, multicentre, placebo-controlled phase II study.* Lancet Oncol, 2007. 8(7): p. 587-94.

112. Bruland, O.S., et al., *High-linear energy transfer irradiation targeted to skeletal metastases by the alpha-emitter 223Ra: adjuvant or alternative to conventional modalities?* Clin Cancer Res, 2006. 12(20 Pt 2): p. 6250s-6257s.

113. Walsh, C.S., *Two decades beyond BRCA1/2: Homologous recombination, hereditary cancer risk and a target for ovarian cancer therapy.* Gynecol Oncol, 2015. 137(2): p. 343-50.

114. Helleday, T., et al., *DNA repair pathways as targets for cancer therapy.* Nat Rev Cancer, 2008. 8(3): p. 193-204.

115. Dillon, M.T., et al., *ATR inhibition potentiates the radiation induced inflammatory tumour microenvironment.* Clin Cancer Res, 2019.

116. Schwartz, J., et al., *Renal uptake of bismuth-213 and its contribution to kidney radiation dose following administration of actinium-225-labeled antibody.* Phys Med Biol, 2011. 56(3): p. 721-33.

117. Yoshida, K., et al., *Pharmacokinetics of single dose radium-223 dichloride (BAY 88-8223) in Japanese patients with castration-resistant prostate cancer and bone metastases.* Ann Nucl Med, 2016. 30(7): p. 453-60.

118. Nilsson, S., et al., *First clinical experience with alpha-emitting radium-223 in the treatment of skeletal metastases.* Clin Cancer Res, 2005. 11(12): p. 4451-9.

10 Appendix 1

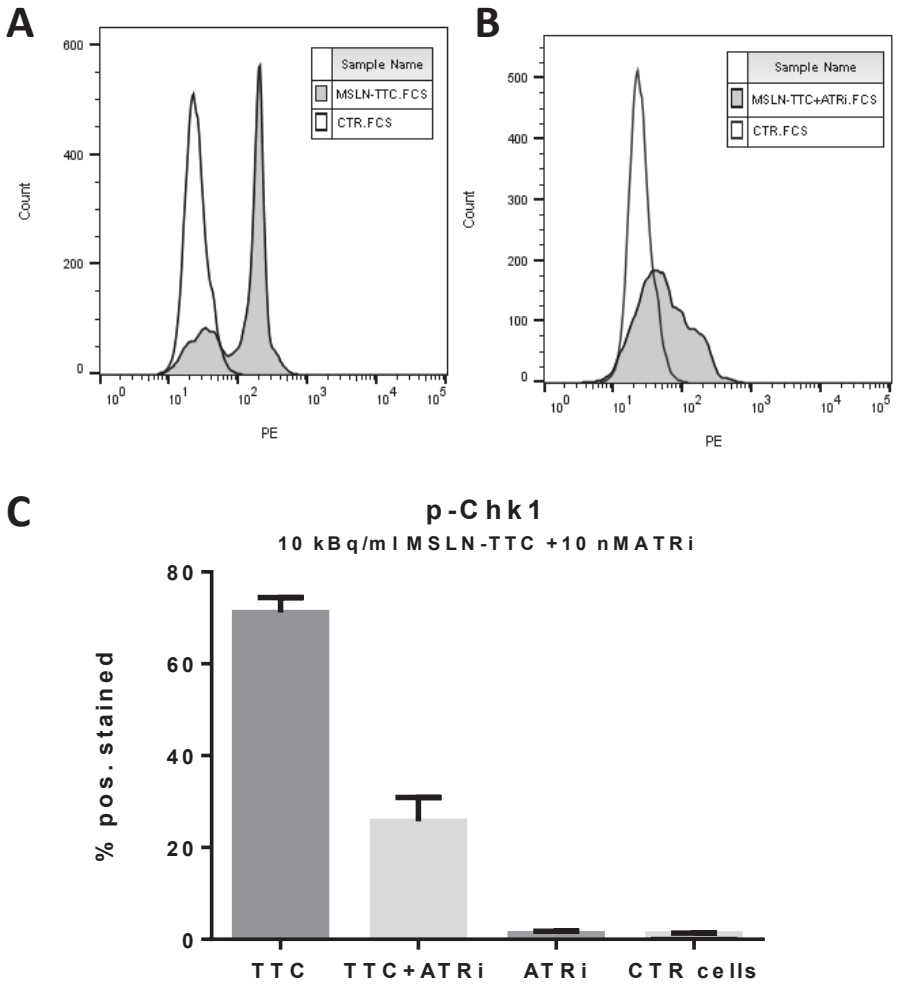

Figure 1 Flow cytometry measurement of p-Chk1 after treatment with MSLN-TTC +/- ATRi. A) Flow cytometry data showing cells stained for p-Chk1 (PE), MSLN-TTC treated cell (gray) as compared to control cells with only secondary PE antibody (white) **B)** Flow cytometry data showing MSLN-TTC+ATRi treated cell (gray) as compared to control cells with only secondary PE antibody (white). **C)** Flow cytometry data shown in A-B presented as % positive cells. The data indicate the suppression of ATR kinase signaling by addition of the ATRi, seen by a reduction in phosphorylated Chk1. Procedure: Seeded cells in 6 well plates and incubated with 10 kBq/ml MSLN-TTC +/- 10 nM ATRi for three days. Cells were fixed and permeabilized using 70 % ice cold ethanol and incubated 1 hour at 4 °C. Cells were resuspended in 100µl anti-p-Chk1 antibody (1:50 in flow buffer, Cat# 133D3, Cell signaling) and 100 µl per well of secondary PE-antibody (1:100 in flow buffer, Cat# 406421, Biolegend, incubated in dark for 1 hour at 4 °C and detection with flow cytometry (Guava Easycyte 8HT).

11 Appendix 2

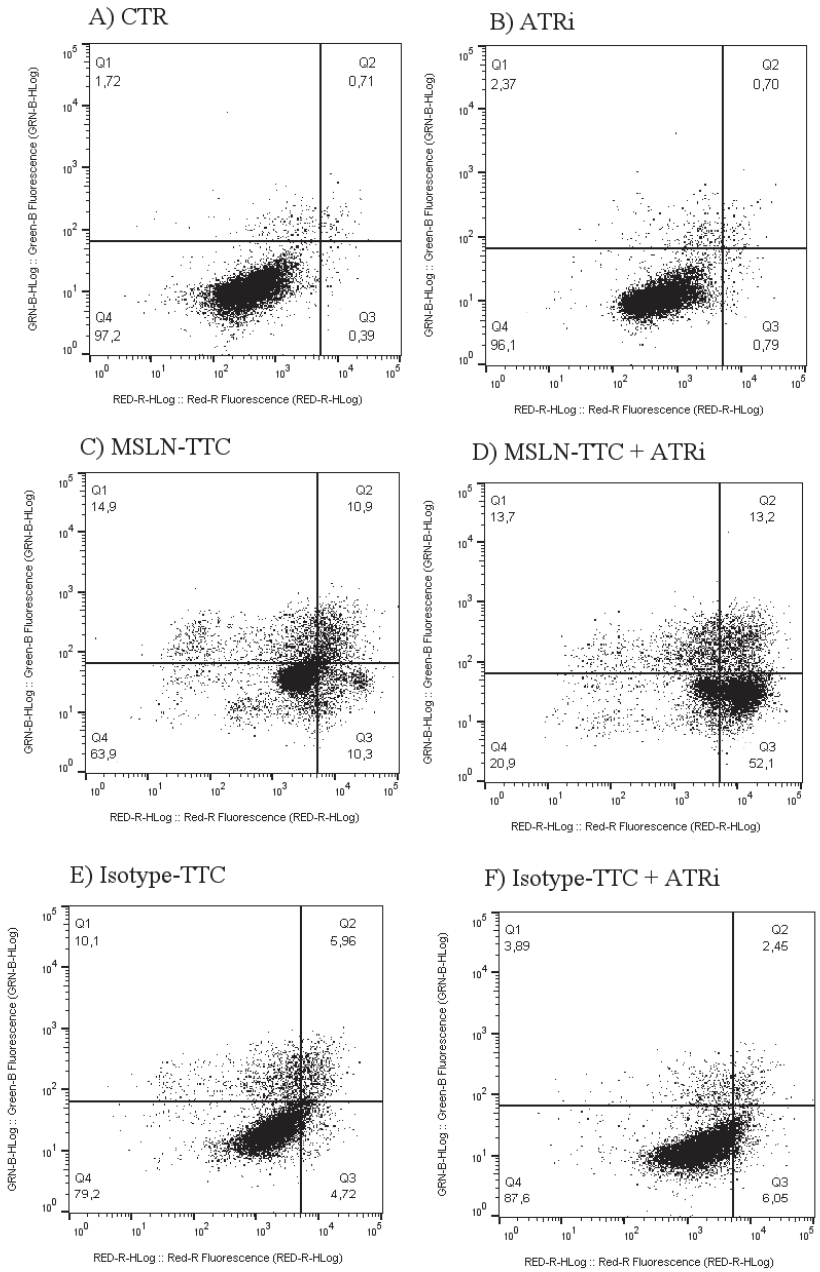

Figure 1 Dot plots showing cells stained for cleaved caspase (Green fluorescence, y-axis) and -H2A.X (Red fluorescence, x-axis) after treatment with TTC +/- ATRi. Seeded cells in 6 well plates and incubated with 20 kBq/ml MSLN-TTC +/- 40 nM ATRi or radiolabelled isotype control +/- 40 nM ATRi for three days. Cells were fixed and permeabilized using 70 % ice cold ethanol and incubated 1 hour at 4 °C. Cells stained as described in section 5.7 and detection with flow cytometry (Guava Easycyte 8HT).

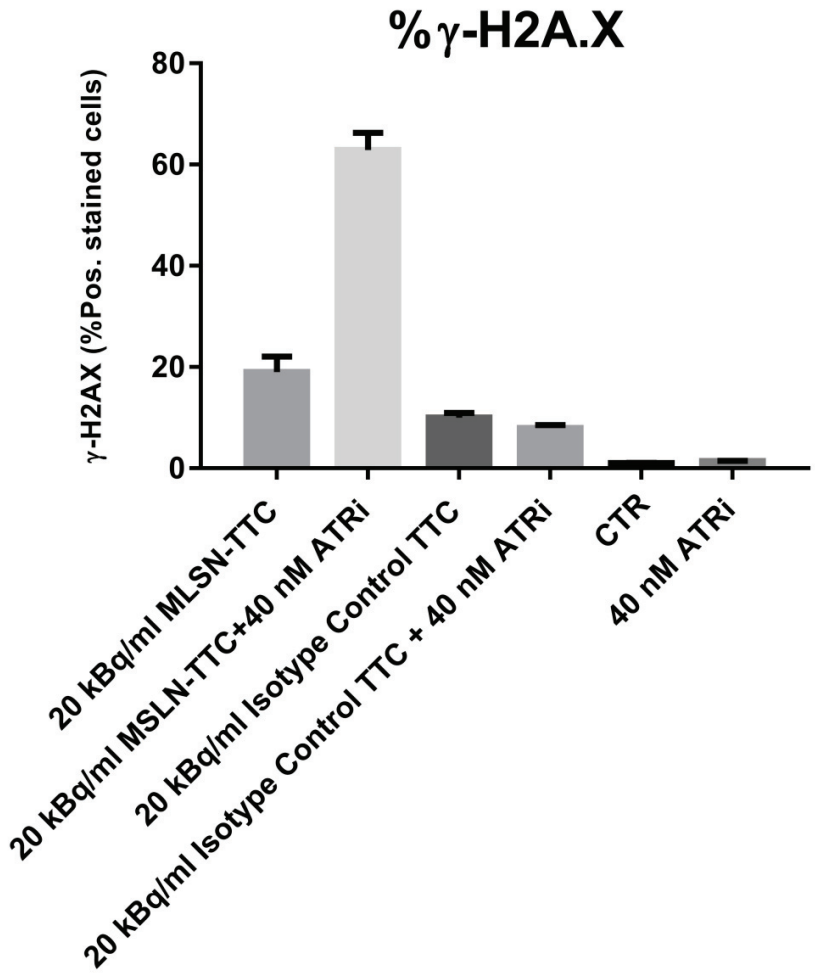

Figure 2: Measurement of double strand DNA breaks (γ-H2A.X). Flow cytometry data as presented in figure 1 plotted as bar charts based on % positive cells.

12 Publications

Paper I

Synergistic Effect of a Mesothelin Targeted Thorium-227 Conjugate in Combination with DNA Damage Response Inhibitors in Ovarian Cancer Xenograft Models

Authors

Katrine Wickstroem[1], Urs B Hagemann[2], Véronique Cruciani[1], Antje M Wengner[2], Alexander Kristian[1], Christine Ellingsen[1], Gerhard Siemeister[2], Roger M Bjerke[1], Jenny Karlsson[1], Olav B Ryan[1], Lars Linden[3], Dominik Mumberg[2], Karl Ziegelbauer[2] and Alan S Cuthbertson[1]

1 Thorium Conjugate Research, Bayer AS, Oslo, Norway

2 Bayer AG, TRG-Oncology II, Berlin, Germany

3 Bayer AG Pharmaceuticals Division, Wuppertal, Germany

Corresponding author: Katrine Wickstroem, PhD student

Mobile: +4741424904, E-mail: katrine.wickstroem@bayer.com

Address: Drammensveien 288, N-0283 Oslo

All authors are employees of Bayer AS or Bayer AG. The work is included in a submitted patent. No other potential conflicts of interest relevant to this article exist.

Word count: 5000

Running title: MSLN-TTC and DDR inhibitors

ABSTRACT

Targeted thorium conjugates (TTCs) represent a new class of therapeutic radiopharmaceuticals for the targeted alpha therapy. They are comprised of the alpha emitter thorium-227 complexed to a 3,2-hydroxypyridinone (3,2-HOPO) chelator conjugated to a tumor targeting monoclonal antibody. The high energy and short range of the alpha particles induce anti-tumor activity, driven by the induction of complex DNA double strand breaks. We hypothesized that blocking the DNA damage response (DDR) pathway should further sensitize cancer cells by inhibiting DNA repair, thereby increasing the response to TTCs. **Methods:** This study reports the evaluation of the mesothelin targeted thorium-227 conjugate (MSLN-TTC; BAY 2287411) in combination with DDR inhibitors, each of them blocking different DDR pathway enzymes. Mesothelin is a validated cancer target known to be overexpressed in mesothelioma, ovarian, lung, breast and pancreatic cancer with low expression in normal tissue. *In vitro* cytotoxicity experiments were performed on cancer cell lines by combining the MSLN-TTC with inhibitors of Ataxia-telangiectasia mutated (ATM), ataxia telangiectasia and Rad3-related (ATR), DNA-dependent protein kinase (DNA-PK), and Poly [ADP-ribose] polymerase 1/2 (PARP1/2). Further, we evaluated the anti-tumor efficacy of the MSLN-TTC in combination with DDR inhibitors in human ovarian cancer xenograft models. **Results:** Synergistic activity was observed *in vitro* for all tested inhibitors when combined with MSLN-TTC. ATRi and PARPi appeared to induce the strongest increase in potency. Further, *in vivo* anti-tumor efficacy of the MSLN-TTC in combination with ATRi or PARPi was investigated in the OVCAR-3 and OVCAR-8 xenograft models in nude mice, demonstrating synergistic anti-tumor activity for the ATRi combination at

doses demonstrated to be non-efficacious when administered as monotherapy. **Conclusion:** The presented data support the mechanism-based rationale for combining the MSLN-TTC with DDR inhibitors as new treatment strategies in MSLN-positive ovarian cancer.

INTRODUCTION

Targeted alpha therapy represents a promising modality whereby the high energy (5-9 MeV) and short range (50-100 µm) of the alpha-particle can be exploited, together with a targeting moiety, to specifically irradiate a tumor while sparing normal tissue (*1,2*). Targeted thorium-227 conjugates (TTCs) comprise the alpha particle emitter thorium-227 complexed to a 3,2-hydroxypyridinone (3,2-HOPO) chelator covalently attached to a tumor-targeting antibody (*3-6*). Thorium-227 has a half-life of 18.7 days and the decay chain deposits five high-energy alpha and two beta particles (*7*). The dense ionization track of the alpha particle induces complex DNA damage both directly and indirectly via generation of reactive oxygen species (*1,8*). In this study, we explore treatment strategies utilizing a mesothelin-targeted thorium-227 conjugate (MSLN-TTC; BAY 2287411) in combination with DNA damage response (DDR) inhibitors. Mesothelin (MSLN) is a 40 kDa membrane-anchored glycoprotein that is frequently overexpressed in cancer types including mesothelioma, ovarian, lung and pancreatic cancers (*9*). In contrast, MSLN has limited expression in nonmalignant tissue and is therefore considered a suitable antigen for targeted therapies (*10-12*). We have previously demonstrated that MSLN-TTC induces specific anti-tumor activity. This agent

is currently in clinical phase I indicated for mesothelioma and ovarian cancer (NCT03507452).

Efficient DNA damage repair is a contributing factor to poor prognosis and treatment outcome following radiotherapy *(13,14*). We therefore hypothesized that DDR pathways also contribute to the efficacy following treatment with MSLN-TTC. This study investigated *in vitro* and *in vivo* combinations of inhibitors of the key mediators of DDR, including Ataxia-telangiectasia mutated (ATM), ataxia telangiectasia and Rad3-related (ATR), DNA-dependent protein kinase (DNA-PK), and Poly [ADP-ribose] polymerase 1/2 (PARP1/2) (*15*) with MSLN-TTC.

MATERIALS AND METHODS

Cells

OVCAR-3, OVCAR-8 from American Type Culture Collection; NCI-H226 from National Institute of Health; Capan-2, HT29 from Deutsche Sammlung von Microorganismen und Zellkulturen GmbH. All cell lines authenticated using PCR fingerprinting. Cells maintained at 37°C, 5% CO_2. Capan-2 and NCI-H226 cultured in Roswell Park Memorial Institute (RPMI) medium. HT29-MSLN in RPMI with 1 % sodium bicarbonate and 2 % hygromycin, OVCAR-3 in RPMI with 10 µg/ml insulin (bovine) and 2 mmol/L glutamine and OVCAR-8 in DMEM/F12. Culture medium was supplemented with 10 % FBS, 1 % penicillin/ streptomycin for all cell lines. HT29 cells transfection with human Mesothelin as described previously (*10*).

Compounds

BAY 1895344 (2-[(3R)-3-methylmorpholin-4-yl]-4-(1-methyl-1H-pyrazol-5-yl)-8-(1H-pyrazol-5-yl)-1,7-naphthyridine) (WO2016020320), PARPi (olaparib), ATMi (AZD0156) and DNA-PKi (VX-984) were synthesized at Bayer AG.

Preparation of the MSLN-TTC

The 3,2-HOPO chelator was conjugated to the MSLN and isotype control antibodies and labeled with thorium-227 as previously described (*4,16*). Antibody-chelator conjugate formulations were incubated with 0.5 – 2.5 MBq thorium-227 at room temperature for 60 min. Radiochemical purity (RCP), defined as the amount of thorium-227 bound to the MSLN-TTC, was determined by instant thin-layer chromatography (iTLC).

In Vitro Experiments

OVCAR-3 cells seeded in 12 (2 ml/well) or 6-well plates (4 ml/well) 24 hours before treatment with MSLN-TTC (1/10 kBq/ml) and ATRi (10 nM) or PARPi (0.5 µM). Due to the half-life of TTC (18.7 d) the cells were exposed to treatment for three days before fixation with 70 % ethanol, followed by staining and detection with Guava Easycyte 8HT. Cell cycle analysis determined by staining with PI/RNase (Cat#F10979, Thermo Fisher), double strand breaks (DSBs) with γH2A.X antibody (Alexa Fluor®-647 Conjugate, Cat# 9720, Cell Signaling Technology) and apoptotic cells with cleaved-caspase-3 antibody (Cat#9669 Alexa Fluor®-488 Conjugate, Cell Signaling Technology). The γH2A.X-positive/ cleaved-caspase-3-negative cells were collected for the determination of DSBs, in order to exclude apoptotic DNA cleavage from the

measurements. Viability was determined after five days exposure by CellTiter Glo (CTG) 2.0 (Cat#G9243, Promega). Data analysis was performed using FlowJo software (version 10) and GraphPad Prism software (version 7).

Combination experiments were conducted in 384-well plates (30 µL/well, 30 000 cells/ml for Capan-2, NCI-H226 and OVCAR-3, 100 000 cells/ml for HT29-MSLN). After 24 hours cells were treated with a titration of MSLN-TTC and DDRi's using a D300e digital dispenser (Tecan) in the following combination ratios with MSLN-TTC (C1) and the DDRi (C2): 1xC1, 0.9xC1+0.1xC2, 0.8xC1+0.2xC2, 0.7xC1+0.3xC2, 0.6xC1+0.4xC2, 0.5xC1+0.5xC2, 0.4xC1+0.6xC2, 0.3xC1+0.7xC2, 0.2xC1+0.8xC2, 0.1xC1+0.9xC2 and 1xC2. MSLN-TTC was titrated in the range 0.001-5 kBq/ml for HT-29-MSLN and 0.01-50 kBq/ml for Capan-2, OVCAR-3/8 and NCI-H226, at a specific activity of 40 kBq ^{227}Th/µg antibody chelator conjugate for HT29-MSLN, Capan-2 and OVCAR-3/8 and 20 kBq ^{227}Th/µg for NCI-H226. DDR inhibitors were dissolved in dimethyl sulfoxide and titrated in the range 0.002-10 µM for ATRi (BAY 1895344), ATMi (AZD0156) or DNA-PKi (VX-984), 0.01-50 µM for PARPi (olaparib/AZD2281). After incubation (HT29-MSLN: 5 days; OVCAR-3/8, NCI-H226 and Capan-2; 7 days) viability was determined using CTG according manufacturer's protocol. Note: optimization for each cell line was required to account for variations in doubling time, receptor density, internalization rates, and radiosensitivity. As a result specific activity, total activity and incubation time vary between the cell lines. IC_{50}-isobolograms were generated by plotting IC_{50} values from MSLN-TTC/ DDRi on x- and y-axis, respectively. The combination index (CI) was determined according to the median-effect model of Chou-

Telalay (*17*), with CI<0.8 defined as synergistic effect, 0.8≤CI≤1.2 defined as additive effect and CI>1.2 defined as antagonistic effect.

***In Vivo* Efficacy**

Experimental protocols were approved by the National Animal Research Authority and conducted according to Federation of European Laboratory Animal Science Association and Directive 2010/63/EU of European Parliament regulations. All animals received an intraperitoneal injection of murine IgG2a antibody (200 µg/animal; UPC10; Sigma) 16-24 hours prior treatment to block nonspecific spleen uptake (*18*). The OVCAR-3-bearing mice were supplemented with 17-beta estradiol either in drinking water (4 mg/L, average daily dose of 1 mg/kg, Sigma-Aldrich, Cat#, E8875) or subcutaneous implantation of pellets (1.7 mg/pellet, time release: 90 days, Innovative Research of America, Cat# SE-121). The tumor growth and the body weights were measured by caliper every second or third day. Animals were sacrificed by cervical dislocation upon reaching the humane endpoint (tumor volume ≥ 1.500 mm^3; body weight loss ≥ 20%).

Five million OVCAR-3 cells in 0.1 ml PBS were inoculated subcutaneously into mice (female, 4-6 weeks old HsdCpb: Athymic nude Foxn1^{nu}, Department for Comparative Medicine, Oslo, Norway, first generation of animals obtained from Harlan, Amsterdam, The Netherlands). At an average tumor area of 25-35 mm^2, the mice (n=10) received a single intravenous (i.v.) injection of MSLN-TTC (100, 250 or 500 kBq/kg, 0.14 mg/kg), isotype-control (250 kBq/kg, 0.14 mg/kg), non-radioactive MSLN antibody-chelator conjugate (0.14 mg/kg) or vehicle. One group was treated with MSLN-TTC (100 kBq/kg, 0.14 mg/kg) and ATRi (40 mg/kg in 60% polyethylene glycol 400/

10% ethanol/ 30% water, 2QD, 3 days on/4 days off, 4 weeks) or PARPi (50 mg/kg in PBS supplemented with 10% 2-HPβCD, daily, 4 weeks). At the study endpoint, tumors treated with MSLN-TTC (500 kBq/kg) and vehicle groups were stained for γH2A.X using rabbit anti-γH2A.X antibody (Milipore, MABE205) with BrightVision rabbit/HRP (Immunologic, DPVR110HRP) incubated for 30 minutes followed by 3,3'-Diaminobenzidine for 5 minutes.

Three million OVCAR-8 cells in 0.1 ml matrigel were inoculated subcutaneously into mice (female, 4-6 weeks old CB-17/Icr-Prkdc^{scid} mice, Janvier, Paris, France). At an average tumor area of 30-40 mm^2, the mice (n=10) received three i.v. injections of MSLN-TTC (200 kBq/kg, 0.14 mg/kg, day 1, 22 and 43) and ATRi (40 mg/kg 2QD, 2 days on/5 days off, seven weeks). Blood samples were collected at end-point of study and analyzed with Hemavet (HV950, Drew Scientific, Inc., Dallas, USA).

To evaluate the cooperativity of combination treatment the expected additivity was calculated according to the Bliss model (*19*)*:* C=A+B-A*B; wherein C is the expected T/C of the combination of drug A and drug B if they act additive, A is T/C of drug A, B is T/C of drug B. Excess >10% over the expected additive effect is assumed to indicate synergism, <10% of the expected additive effect is assumed antagonism.

Statistics

Statistical significance was evaluated using GraphPad Prism software (version 7.0) applying student t-test and one-way ANOVA followed by Tukey's test.

RESULTS

Preparation and Characterization of MSLN-TTC

Radiolabeling was effected by incubation of thorium-227 with the antibody conjugate at ambient temperatures (*3,4,6*). The RCP was determined by iTLC for each experiment and was consistently ≥ 95 %. The binding affinity was not impaired by conjugation or radiolabeling (Supplemental Figs. 1 and 2).

Synergistic Effect of MSLN-TTC and DDR Inhibitors *In Vitro*

In vitro cytotoxicity experiments were performed on cell lines of different tissue origin and MSLN expression (see table 1). The effect of the combination was evaluated by isobolograms as exemplified in Fig. 1 for the OVCAR-3 cell line and Supplemental Figs. 3-6. Data analysis according to the median-effect model of Chou-Telalay gave combination indexes indicating synergistic, additive and antagonistic effects *(17).* All DDR inhibitors demonstrated synergy in combination with MSLN-TTC in the OVCAR-3 cell line (table 1). Furthermore, the ATRi induced strongest synergy in combination with MSLN-TTC in all tested cell lines. In contrast, the synergistic effect was not as well pronounced for ATMi or DNA-PKi, which induced both additive and antagonistic effects.

ATRi and PARPi Potentiate MSLN-TTC Activity by Suppressing DNA Damage Repair

Based on the robust synergy observed *in vitro* we investigated the mechanism of combination treatment in the OVCAR-3 model to determine whether the enhanced effect correlated with inhibition of DNA damage repair.

DSBs and cell cycle arrest in G2 or M phase was observed evidenced by increased γH2A.X and accumulation of cells with 4N DNA content respectively in cells treated with a single sub-lethal dose of MSLN-TTC. When combined with a non-efficacious dose of ATRi (10 nM), the percentage of cells entering the G2/M cell cycle phase was reduced. In contrast the number of γH2A.X positive cells increased (Figs. 2A and 2B; Supplemental Table 1) correlating with a higher level of apoptosis and decrease in cell viability, demonstrating the potency of the combination (Supplemental Figs. 7A and 7B; Supplemental Table 1). When MSLN-TTC was combined with a non-efficacious dose of PARPi (0.5 μM) we observed an increase in cell cycle arrest and γH2A.X (Figs. 2C and 2D; Supplemental Table 2). This translated to a modest increase in potency of MSLN-TTC as determined by viability assay and increase in apoptosis (Supplemental Figs. 7C and 7D; Supplemental Table 2), although to a lesser extent than in the combination with ATRi.

Tumor Growth Inhibition of MSLN-TTC in the OVCAR-3 Ovarian Cancer Xenograft Model

The *in vivo* efficacy was determined by measuring changes in tumor area after administration of a single dose of MSLN-TTC at 100, 250 and 500 kBq/kg. An isotype control (250 kBq/kg) was included for comparison. Statistically significant tumor growth inhibition compared to vehicle was achieved for the MSLN-TTC at 250 and 500 kBq/kg

(p< 0.0001) the highest dose resulting in a more pronounced reduction in tumor size (Fig. 3A). No statistical significance was observed for the dose of 100 kBq/kg of MSLN-TTC or for the isotype control versus the vehicle control group. IHC analysis of γH2A.X on tumor tissue demonstrated induction of a higher level of DSBs compared to vehicle control after treatment with MSLN-TTC (500 kBq/kg) (Fig. 3B).

Enhanced Potency of MSLN-TTC in Combination with ATRi or PARPi in OVCAR-3 and OVCAR-8

Based on the observed synergistic effect of MSLN-TTC in combination with ATRi and PARPi *in vitro*, we further evaluated the *in vivo* efficacy of both combinations in an OVCAR-3 xenograft model. Since a single dose of 250 kBq/kg was highly efficacious as a monotherapy, we selected the lower dose of 100 kBq/kg for the combination study. ATRi was dosed one week after MSLN-TTC at 40 mg/kg 2QD, three days on/four days off, for four weeks and PARPi at 50 mg/kg daily for four weeks based on internal and published data respectively *(20)*. Results from biodistribution studies show that TTCs typically accumulate in tumors over four-seven days and have extensive retention (*4,5*). Given the 18.7 days half-life of thorium-227, the absorbed dose to tumor is delivered over several weeks. Thus, DDR inhibitors are administered over a four week period as more DNA damage is induced over time by the TTC.

The ATRi combination enhanced the potency of the MSLN-TTC with significant tumor growth inhibition compared to the vehicle control (P< 0.0001) and monotherapy groups (p<0.01) (Fig. 4A). Furthermore, the combination effect was determined to be synergistic based on the Bliss model (*19*). Although the PARPi combination was

efficacious compared to the vehicle group, significance was not achieved when compared to the respective MSLN-TTC monotherapy, the combination effect was determined to be additive (Fig. 4B). Both dosing schedules were well tolerated as evidenced by the stable body weights in all groups tested (Supplemental Fig. 8).

We further explored the combination of MSLN-TTC and ATRi in the OVCAR-8 ovarian cancer xenograft model, which had previously demonstrated *in vitro* synergy from the ATRi combination (Supplemental Fig. 6). Due to lower receptor-level and a more rapid growth rate the dosing schedule was changed to 3 x 200 kBq/kg MSLN-TTC and ATRi (40 mg/kg, 2QD, 2 days on/ 5 days off). There was a significant effect of monotherapy with MSLN-TTC or ATRi compared to vehicle treated control in the OVCAR-8 model ($P<0.0001$). The combination induced a significantly enhanced anti-tumor effect as compared to the monotherapy ($p< 0.001$) (Fig. 5A) which was synergistic. No significant change in body weight was observed in any of the treatment groups (Supplemental Fig. 8). However, a significant reduction in white blood cells (WBCs) ($P<0.001$) and platelets ($P<0.001$) was observed for MSLN-TTC monotherapy and the ATRi combination (Fig. 5B) in comparison to vehicle control. The reduction in WBCs and platelets was comparable for MSLN-TTC and the combination, indicating no combined toxicity effect at the timepoint evaluated.

DISCUSSION

Several clinical and preclinical studies support the synergistic effects of combining targeted drugs with radiation therapy for the treatment of solid tumors (*21*). Drug combinations have the potential to sensitize tumor cells to ionizing radiation, enhancing the therapeutic effect while minimizing side effects and damage to normal tissue. We report herein the pre-clinical evaluation of a combination of inhibitors of DNA damage repair with systemic targeted alpha therapy. As the mode of action of targeted alpha therapy is based on the induction of complex DNA damage, we postulated that combinations with DDR inhibitors may induce synergistic effect. Alpha particles are considered to be highly cytotoxic due to extensive induction of DSBs and the development of radio-resistance has not been reported for alpha particle therapy (*22,23*). In contrast, low linear energy transfer (LET) particles or rays, induce sublethal damage such as single strand breaks (SSBs), which cells have a higher capacity to repair by e.g. excision repair mechanisms (*24*). In the present study, a mesothelin specific antibody-chelator conjugate was prepared using the fully human anti-mesothelin antibody anetumab. The antibody binds specifically to MSLN with high affinity (K_D of 14 nM) and induces efficient internalization on MSLN expressing cell lines.

We initially screened for synergistic effects of MSLN-TTC and DDR inhibitors in viability assays. The MSLN-TTC was shown to synergize with all DDR inhibitors tested (ATMi, ATRi, DNA-PKi and PARPi) while a more pronounced effect was observed for ATRi and PARPi. Mechanistic studies evaluating the ATRi combination on OVCAR-3 cells revealed a significantly higher proportion of cells continuing through the cell cycle into G1/S phase than for the MSLN-TTC monotherapy ($p < 0.0001$). The reduced level

of cell cycle arrest for the ATRi combination can be explained by the blockage of the ATR kinase at the G2 cell cycle checkpoint (*25*). It also appeared that this combination resulted in a higher level of DSBs as evidenced by γ-H2A.X staining. Furthermore, the potency of the combination was reflected in an increase in apoptosis and reduction in cell viability. In contrast, the PARPi combination appeared to increase cell cycle arrest and γ-H2A.X staining was less pronounced, as was induction of apoptosis markers and cell viability. The cell cycle data therefore appear to reflect key mechanistic differences between ATR, involved in cell cycle arrest and DNA DSB repair and PARP, involved in single strand repair.

Ovarian cancer is an indication with unmet medical need and is a preferred indication for the MSLN-TTC clinical study. Based on the strong *in vitro* synergy on the ovarian cancer cell line OVCAR-3, we chose this model for *in vivo* evaluation of the combinations of MSLN-TTC with the PARPi and the ATRi. First, a dose response study was performed in OVCAR-3 tumor bearing mice treated with a single dose of 100, 250 or 500 kBq/kg of MSLN-TTC. Significant inhibition of tumor growth was measured at 250 and 500 kBq/ kg, while 100 kBq/kg gave no measurable effect on growth inhibition compared to vehicle control. Non-significant efficacy was observed for the isotype control at 250 kBq/kg, which is likely to arise from non-target mediated enhanced permeability and retention effect (*26*). IHC analysis of γH2A.X indicated higher levels of DSBs in the 500 kBq/ kg group compared to vehicle controls further supporting the validity of testing the DDR inhibitor combination in this model at lower doses.

When MSLN-TTC was combined with the PARPi at a single dose of 100 kBq/kg, statistical significance was achieved when compared to the vehicle control ($P<0.001$).

However, the PARPi combination was not significantly different to the 100 kBq/kg monotherapy treatment. This lack of *in vivo* synergy may serve to highlight that inhibition of SSB repair, mediated by PARP, has a less pronounced effect than targeting DSB repair and cell cycle checkpoint, mediated by ATR, in the response to alpha-radiation induced DNA damage. In contrast, MSLN-TTC combined with ATRi (40 mg/kg) at a single dose of 100 kBq/kg, resulted in a more pronounced tumor growth inhibition in comparison to the combination with PARPi. The combination induced significant ($p<0.001$) tumor growth inhibition, the level of this effect being equivalent to the single dose of 250 kBq/kg of MSLN-TTC, and was determined to be strongly synergistic by the Bliss additivity model. This is in alignment with our observations from the *in vitro* studies and further supports the hypothesis that blockage of the DNA double strand break repair machinery results in stronger therapeutic efficacy. Further studies need to be performed in order to investigate the effect of alternative dosing schedules.

A second human ovarian cancer xenograft model using the OVCAR-8 cell line was selected for further evaluation of the ATRi combination. This model had a lower level of receptors and a more rapid growth rate. The dosing regimen was therefore changed to 3 x 200 kBq/kg administered as monotherapy or in combination with ATRi (40 mg/kg 2QD, 2 days on/ 5 days off)**.** Each single agent (MSLN-TTC or ATRi) induced a significant tumor growth inhibition ($p<0.0001$) compared to vehicle. However, the combination resulted in a significant increase of tumor growth inhibition compared to both monotherapies ($p<0.001$), demonstrating the synergistic activity. All doses were well tolerated as evidenced by no critical body weight loss. Hematological analysis

showed comparable values of MSLN-TTC monotreatment and the combination with ATRi, indicating that there was no increased toxicity from the combination treatment.

In summary, these findings demonstrate that the combination effect appears to be DDR pathway dependent. The ATRi has been reported to induce synthetic lethality in tumors with defects in G1 cell cycle checkpoint, including mutations in ATM and TP53 (*25*). Interestingly, the monotherapy with ATRi was more efficacious in the OVCAR-8 model (ATM^{mut}/ $TP53^{mut}$), inducing a significant tumor growth inhibition in comparison to the OVCAR-3 model ($TP53^{mut}$) (*27*). The mutations may have contributed to the enhanced efficacy of the ATRi treatment in the OVCAR-8 model as ATM defects has been describe to make cells more dependent on ATR. However, as these models are not sufficiently comparable a broader assessment of the therapeutic relevance of targeting specific mutations in relation to synergy in pre-clinical models will be the subject of future work. It also remains to be explored if the synergy of MSLN-TTC/PARPi combinations can be enhanced in tumors characterized with BRCA1/2 defects, as the PARP/BRCA combination is well described to induce synthetic lethality (*28*).

CONCLUSION

The presented study supports the rationale for combining the MSLN-TTCs with DDR inhibitors based on their individual mode of action as a new strategy for treating ovarian cancer patients characterized by overexpression of mesothelin.

ACKNOWLEDGEMENTS

We would like to thank the Research Council of Norway for funding this study. Further, we would like to thank Nils Guthof and Lisa Ehresmann for excellent technical assistance in conducting the OVCAR-8 study.

KEY POINTS

Question: As the mechanism of action of MSLN-TTC is primarily linked to induction of DNA damage we hypothesized that combinations with DNA damage response (DDR) inhibitors would induce synergistic effect and improved treatment outcome at lower doses.

Pertinent finding: *In vitro* evaluation demonstrated synergistic effect of MSLN-TTC in combination with inhibitors of ATR, ATM, DNA-PK and PARP. In addition, *in vivo* studies demonstrated significantly enhanced anti-tumor efficacy and synergy of MSLN-TTC and ATRi combination in ovarian cancer xenografts at dose levels shown to be non-efficacious when administered as monotherapies.

Implication for patient care: The presented study supports the rationale for combining the MSLN-TTCs with DDR inhibitors based on their individual mode of action as a new strategy for treating ovarian cancer patients characterized by overexpression of mesothelin.

REFERENCES

1. Sgouros G, Roeske JC, McDevitt MR, et al. MIRD pamphlet no. 22 (abridged): radiobiology and dosimetry of alpha-particle emitters for targeted radionuclide therapy. *J Nucl Med*. 2010;51:311-28

2. Parker C, Lewington V, Shore N, et al. Targeted alpha therapy, an emerging class of cancer agents: a review. *JAMA Oncol.* 2018;4:1765-1772.

3. Ramdahl T, Bonge-Hansen HT, Ryan OB, et al. An efficient chelator for complexation of thorium-227. *Bioorg Med Chem Lett*. 2016;26:4318-21.

4. Hagemann UB, Mihaylova D, Uran SR, et al. Targeted alpha therapy using a novel CD70 targeted thorium-227 conjugate in in vitro and in vivo models of renal cell carcinoma. *Oncotarget*. 2017; 8:56311-56326.

5. Hagemann UB, Wickstroem K, Wang E, et al. In vitro and in vivo efficacy of a novel CD33-targeted thorium-227 conjugate for the treatment of acute myeloid leukemia. *Mol Cancer Ther*. 2016;15:2422-31.

6. Deblonde GJ, Lohrey TD, Booth CH, et al. Solution thermodynamics and kinetics of metal complexation with a hydroxypyridinone chelator designed for thorium-227 targeted alpha therapy. *Inorg Chem*. 2018;57:14337-14346.

7. Henriksen G, Fisher DR, Roeske JC, et al. Targeting of osseous sites with alpha-emitting 223Ra: comparison with the beta-emitter 89Sr in mice. *J Nucl Med*. 2003;44:252-9.

8. Carter RJ, Nickson CM, Thompson JM, et al. Complex DNA damage induced by high linear energy transfer alpha-particles and protons triggers a specific cellular DNA damage response. *Int J Radiat Oncol Biol Phys*. 2018;100:776-84.

9. Hassan R, Ho M. Mesothelin targeted cancer immunotherapy. *Eur J Cancer*. 2008;44:46-53.

10. Golfier S, Kopitz C, Kahnert A, et al. Anetumab ravtansine: a novel mesothelin-targeting antibody-drug conjugate cures tumors with heterogeneous target expression favored by bystander effect. *Mol Cancer Ther*. 2014;13:1537-48.

11. Quanz M, Hagemann UB, Zitzmann-Kolbe S, et al. Anetumab ravtansine inhibits tumor growth and shows additive effect in combination with targeted agents and chemotherapy in mesothelin-expressing human ovarian cancer models. *Oncotarget*. 2018;9:34103-21.

12. Hassan R, Bera T, Pastan I. Mesothelin: a new target for immunotherapy. *Clin Cancer Res*. 2004;10:3937-42.

13. Harrington K, Jankowska P, Hingorani M. Molecular biology for the radiation oncologist: the 5Rs of radiobiology meet the hallmarks of cancer. *Clin Oncol (R Coll Radiol)*. 2007;19:561-71.

14. Rosser CJ, Gaar M, Porvasnik S. Molecular fingerprinting of radiation resistant tumors: can we apprehend and rehabilitate the suspects? *BMC Cancer*. 2009;9:225.

15. Huhn D, Bolck HA, Sartori AA. Targeting DNA double-strand break signalling and repair: recent advances in cancer therapy. *Swiss Med Wkly*. 2013;143:w13837.

16. Abbas N, Heyerdahl H, Bruland OS, et al. Experimental alpha-particle radioimmunotherapy of breast cancer using 227Th-labeled p-benzyl-DOTA-trastuzumab. *EJNMMI Res*. 2011;1:18.

17. Chou TC. Theoretical basis, experimental design, and computerized simulation of synergism and antagonism in drug combination studies. *Pharmacol Rev*. 2006;58:621-81.

18. Reddy N, Ong GL, Behr TM, et al. Rapid blood clearance of mouse IgG2a and human IgG1 in many nude and nu/+ mouse strains is due to low IgG2a serum concentrations. *Cancer Immunol Immunother.* 1998;46:25-33.

19. Bliss CI. The toxicity of poisons applied jointly. *Ann Appl Biol*. 1939:585-615.

20. Senra JM, Telfer BA, Cherry KE, et al. Inhibition of PARP-1 by olaparib (AZD2281) increases the radiosensitivity of a lung tumor xenograft. *Mol Cancer Ther*. 2011;10:1949-58.

21. Selzer E, Kornek G. Targeted drugs in combination with radiotherapy for the treatment of solid tumors: current state and future developments. *Expert Rev Clin Pharmacol*. 2013;6:663-76.

22. Baidoo KE, Yong K, Brechbiel MW. Molecular pathways: targeted alpha-particle radiation therapy. *Clin Cancer Res*. 2013;19:530-7.

23. Haro KJ, Scott AC, Scheinberg DA. Mechanisms of resistance to high and low linear energy transfer radiation in myeloid leukemia cells. *Blood*. 2012;120:2087-97.

24. Pouget JP, Navarro-Teulon I, Bardies M, et al. Clinical radioimmunotherapy - the role of radiobiology. *Nat Rev Clin Oncol*. 2011;8:720-34.

25. Dillon MT, Good JS, Harrington KJ. Selective targeting of the G2/M cell cycle checkpoint to improve the therapeutic index of radiotherapy. *Clin Oncol (R Coll Radiol)*. 2014;26:257-65.

26. Maeda H, Nakamura H, Fang J. The EPR effect for macromolecular drug delivery to solid tumors: improvement of tumor uptake, lowering of systemic toxicity, and distinct tumor imaging in vivo. *Adv Drug Deliv Rev*. 2013;65:71-9.

27. COSMIC: somatic cancer genetics at high-resolution: *cancer.sanger.ac.uk, Accessed Jan 15, 2019*.

28. Fong PC, Boss DS, Yap TA, et al. Inhibition of poly(ADP-ribose) polymerase in tumors from BRCA mutation carriers. *N Engl J Med*. 2009;361:123-34.

Figure 1. Synergistic effect of MSLN-TTC and DDRis on ovarian cancer cell line OVCAR-3. IC_{50}-isobolograms with MSLN-TTC and A) ATMi AZD0156, B) ATRi BAY 1895344, C) DNA-PKi VX-984 and D) PARPi olaparib on OVCAR-3 cells. Combination index (CI) (mean, n=3) was determined according to the median-effect model of Chou-Telalay, CI<0.8 defined as synergistic effect, 0.8<CI>1.2 defined as additive effect and CI>1.2 defined as antagonistic effect.

Figure 2. *In vitro* mechanistic experiments from MSLN-TTC +/- ATRi BAY 1895344 or PARPi olaparib on OVCAR-3. A) Cell cycle analysis and B) γ–H2A.X determined after treatment with MSLN-TTC (10 kBq/ml) and ATRi (10 nM) for three days. C) Cell cycle analysis and D) γ–H2A.X determined after treatment with MSLN-TTC (1 kBq/ml) and PARPi (0.5 μM) for three days. Error bars represent SD of mean, n=3.

Figure 3. *In vivo* characterization of monotreatment with MSLN-TTC in OVCAR-3 xenograft model. A) Tumor size determined after a single dose (100, 250 or 500 kBq/kg, 0.14 mg/kg, i.v.) of MSLN-TTC, isotype control (250 kBq/kg, 0.14 mg/kg, i.v.) or vehicle control. Statistical analysis was performed using one-way ANOVA followed by Tukey's test. ****, $P < 0.0001$. B) IHC of γH2A.X on tumors after a single dose (500 kBq/kg, 0.14 mg/kg, i.v.) of MSLN-TTC or vehicle control.

Figure 4. *In vivo* efficacy of MSLN-TTC in combination with ATRi or PARPi in the OVCAR-3 xenograft model. A) Tumor size determined after a single dose of MSLN-TTC (100 kBq/kg, 0.14 mg/kg, i.v.) and ATRi (40 mg/kg 2QD, 3 days on/ 4 days off, 4 weeks) and B) Tumor size determined after a single dose of MSLN-TTC (100 kBq/kg, 0.14 mg/kg, i.v.) and PARPi (50 mg/kg QD,4 weeks). Statistical analysis was performed

using one-way ANOVA followed by Tukey's test. **, P < 0.01; ***, P < 0.001; ****, P < 0.0001. T/C: treatment-to-control ratio

Figure 5. *In vivo* efficacy of MSLN-TTC in combination with ATRi in the OVCAR-8 xenograft model. A) Tumor size and B) WBCs and platelets determined at the end-point of study after three (i.v.) injections of MSLN-TTC (200 kBq/kg, 0.14 mg/kg) and ATRi (40 mg/kg 2QD, 2 days/5 days off). Statistical analysis was performed using one-way ANOVA followed by Tukey's test. ***, P < 0.001, ****,P<0.0001, T/C: treatment-to-control ratio.

Table 1. *In vitro* characterization of MSLN-TTC and DDR

Cell line, cancer type	Antibodies bound per cell	Monotreatment MSLN-TTC, IC_{50}(kBq/mL)	Monotreatment DDRis, IC_{50}(nM)				Combination index (CI)			
			ATMi	ATRi	DNA-PKi	PARPi	+ATMi*	+ATRi*	+DNA-PKi*	+PARPi*
NCI-H226, Lung/mesothelioma	2 000	2.0	0.2	10	90	200	0.9±0.2$^{(add)}$	0.5±0.1$^{(s)}$	0.7±0.1$^{(s)}$	0.8±0.1$^{(add)}$
Capan-2, pancreatic cancer	20 000	28	40	70	16	19	1.1±0.1$^{(add)}$	0.6±0.2$^{(s)}$	1.2±0.1$^{(ant)}$	1.0±0.1$^{(add)}$
OVCAR-3, ovarian cancer	60 000	2.5	0.3	60	90	1.4	0.7±0.1$^{(s)}$	0.4±0.04$^{(s)}$	0.7±0.2$^{(s)}$	0.5±0.1$^{(s)}$
OVCAR-8, ovarian cancer	40 000	3.0	ND	120	ND	ND	ND	0.7±0.1$^{(s)}$	ND	ND
HT29-MSLN, colorectal cancer	240 000	0.2	400	60	30	200	1.4±0.3$^{(ant)}$	0.7±0.1$^{(s)}$	0.9±0.4$^{(add)}$	0.6±0.1$^{(s)}$

IC50, half maximal inhibitory concentration; CI, combination index, ND: not determined; CI-data presented as mean ±SD, n=3,
* In combination with MSLN-TTC. $^{(add)}$ = additive, $^{(ant)}$ = antagonistic, $^{(s)}$ = synergistic

Figure 1.

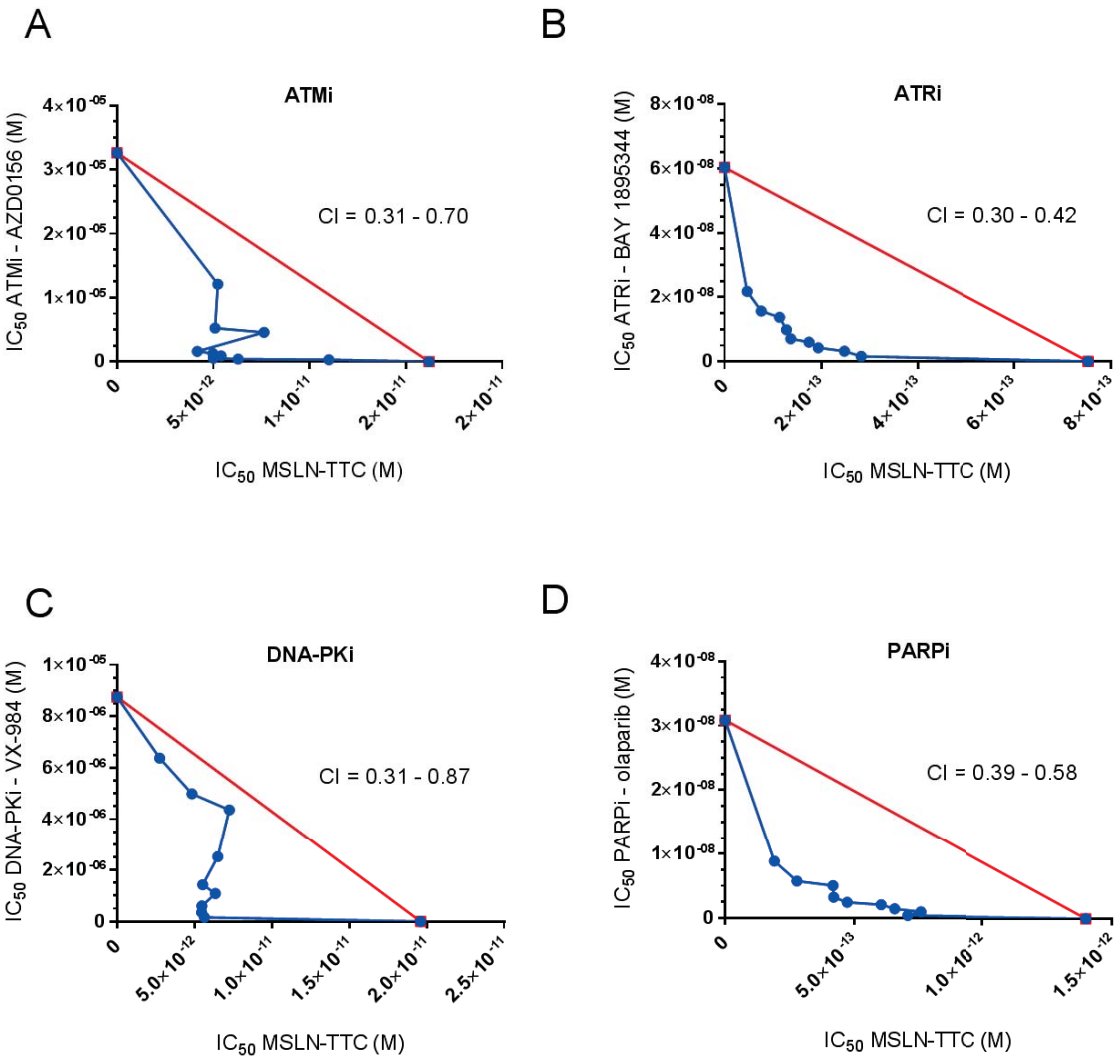
A
ATMi
CI = 0.31 - 0.70
IC50 ATMi - AZD0156 (M)
IC50 MSLN-TTC (M)
B
ATRi
CI = 0.30 - 0.42
IC50 ATRi - BAY 1895344 (M)
IC50 MSLN-TTC (M)
C
DNA-PKi
CI = 0.31 - 0.87
IC50 DNA-PKi - VX-984 (M)
IC50 MSLN-TTC (M)
D
PARPi
CI = 0.39 - 0.58
IC50 PARPi - olaparib (M)
IC50 MSLN-TTC (M)

Figure 2.

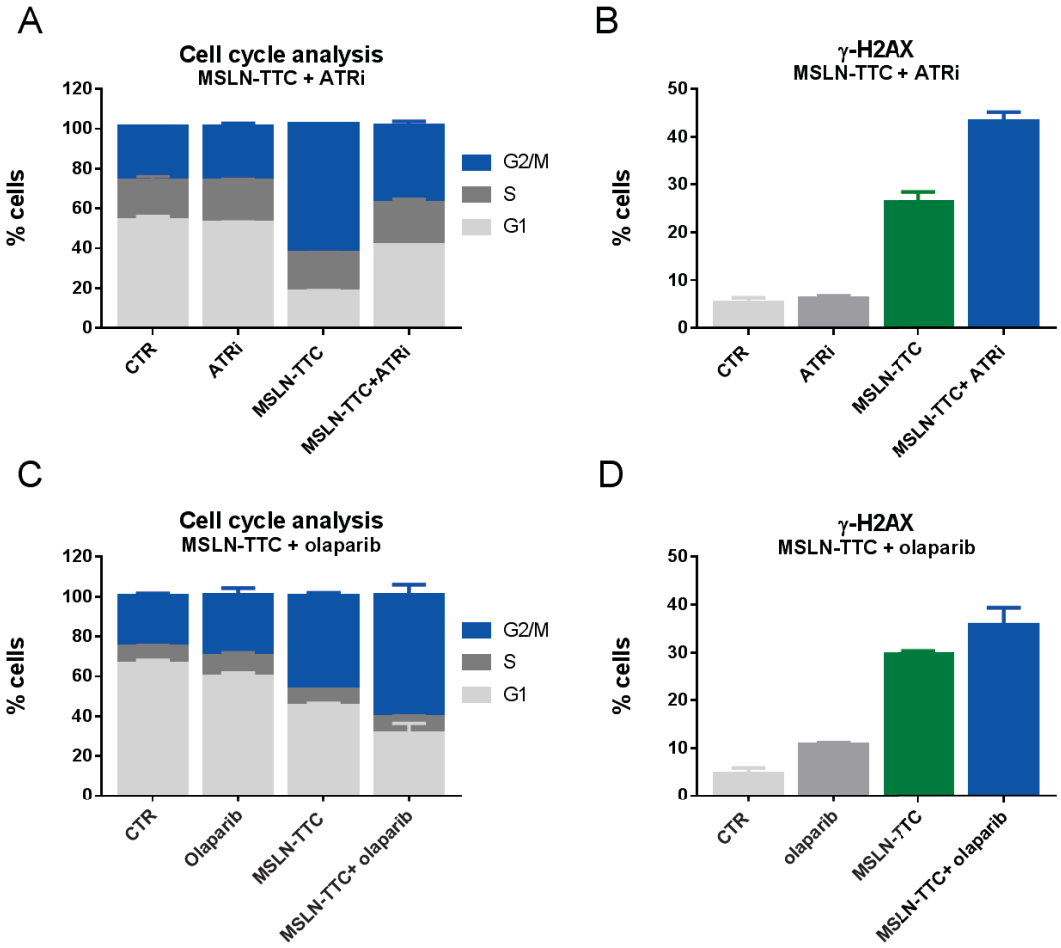
A
Cell cycle analysis
MSLN-TTC + ATRi
% cells
120
100
80
60
40
20
0
G2/M
S
G1
CTR
ATRi
MSLN-TTC
MSLN-TTC+ATRi
B
γ-H2AX
MSLN-TTC + ATRi
% cells
50
40
30
20
10
0
CTR
ATRi
MSLN-TTC
MSLN-TTC+ ATRi
C
Cell cycle analysis
MSLN-TTC + olaparib
% cells
120
100
80
60
40
20
0
G2/M
S
G1
CTR
Olaparib
MSLN-TTC
MSLN-TTC+ olaparib
D
γ-H2AX
MSLN-TTC + olaparib
% cells
50
40
30
20
10
0
CTR
olaparib
MSLN-TTC
MSLN-TTC+ olaparib

Figure 3.

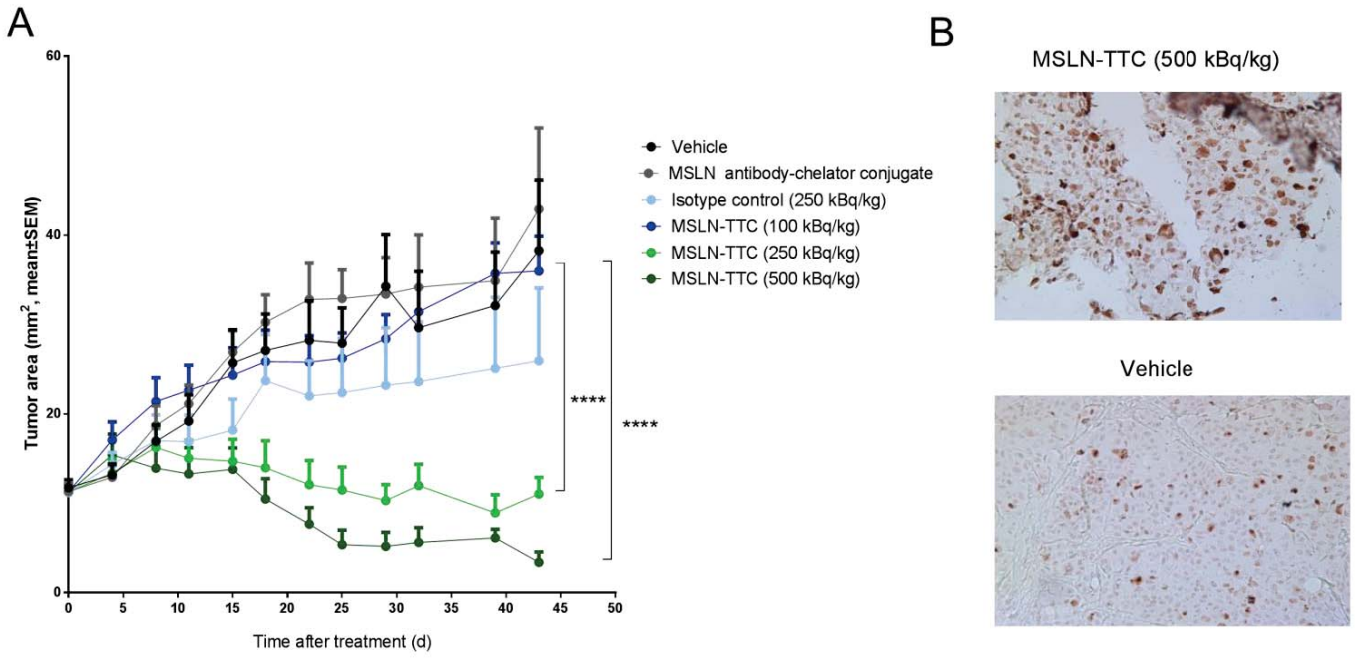
A
B
Tumor area (mm^2, mean±SEM)
Time after treatment (d)
Vehicle
MSLN antibody-chelator conjugate
Isotype control (250 kBq/kg)
MSLN-TTC (100 kBq/kg)
MSLN-TTC (250 kBq/kg)
MSLN-TTC (500 kBq/kg)
****
****
MSLN-TTC (500 kBq/kg)
Vehicle

Figure 4.

A

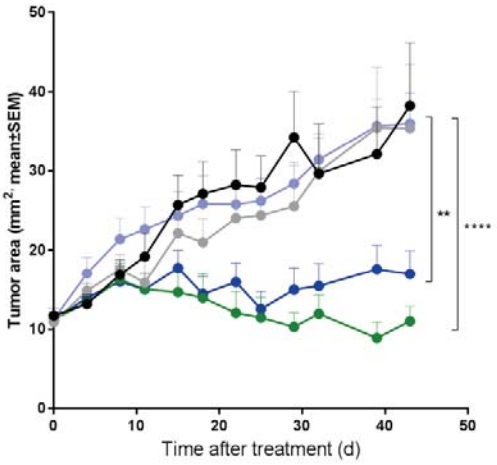

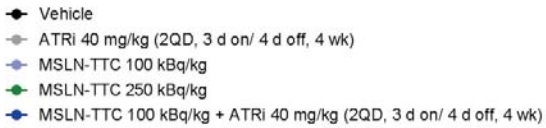

	T/C (%)	Inhibition (%)	Calculated combined response (%)	Excess over Bliss additivity (%)
ATRi	92.0	8.0	0.08	NA
MSLN-TTC	94.0	6.0	0.06	NA
MSLN-TTC+ ATRi	44.0	56.0	0.14	314

B

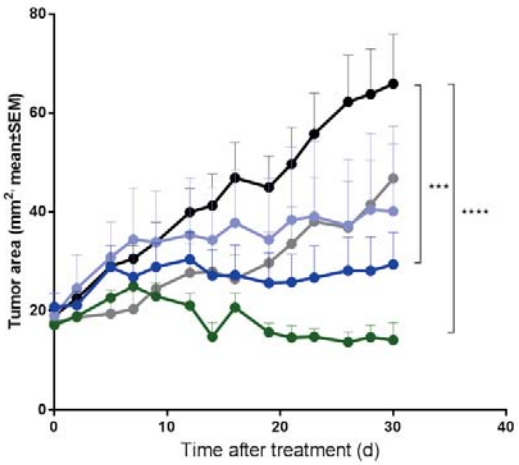

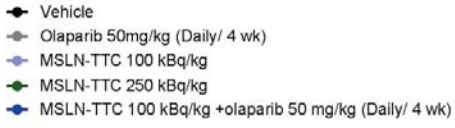

	T/C (%)	Inhibition (%)	Calculated combined response (%)	Excess over Bliss additivity (%)
Olaparib	70.0	30.0	0.30	NA
MSLN-TTC	61.0	39.0	0.39	NA
MSLN-TTC+ olaparib	44.0	56.0	0.57	-2

Figure 5.

A

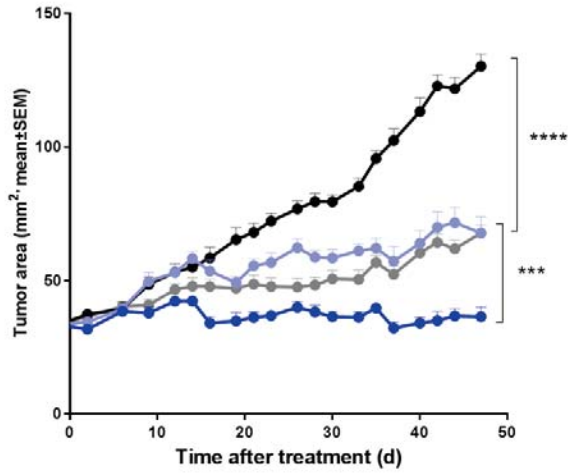

	T/C (%)	Inhibition (%)	Calculated combined response (%)	Excess over Bliss additivity (%)
ATRi	35.0	65.0	0.65	NA
MSLN-TTC	36.0	64.0	0.64	NA
MSLN-TTC+ ATRi	0.3	99.7	0.87	14

B

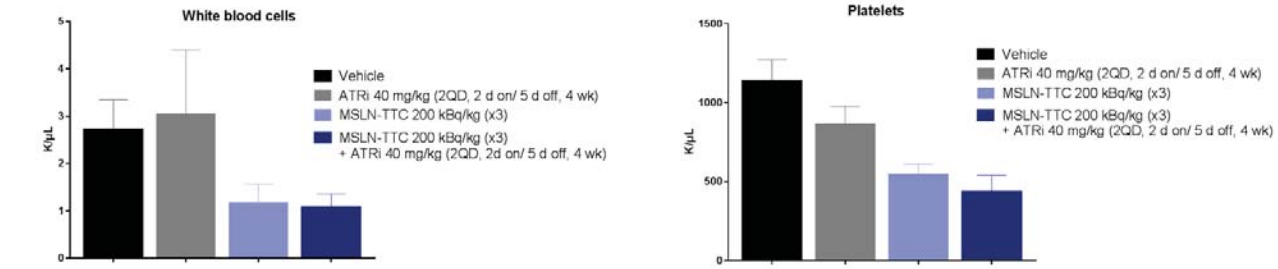

Supporting Information for:

"Synergistic Effect of a Mesothelin Targeted Thorium-227 Conjugate in Combination with DNA Damage Response Inhibitors in Ovarian Cancer Xenograft Models"

Authors

Katrine Wickstroem[1], Urs B Hagemann[2], Véronique Cruciani[1], Antje M Wengner[2], Alexander Kristian[1], Christine Ellingsen[1], Gerhard Siemeister[2], Roger M Bjerke[1], Jenny Karlsson[1], Olav B Ryan[1], Lars Linden[3], Dominik Mumberg[2], Karl Ziegelbauer[2] and Alan S Cuthbertson[1]

1 Thorium Conjugate Research, Bayer AS, Oslo, Norway

2 Bayer AG, TRG-Oncology II, Berlin, Germany

3 Bayer AG Pharmaceuticals Division, Wuppertal, Germany

Figure 1: FACS Analysis Comparing Binding Potency of MSLN-antibody Conjugate

Cells were seeded in 96 well plates (100 000 cells, 100 µl) and incubated with a titration of 0.0006-100 µg/ml of anti-MSLN antibody, MSLN-antibody conjugate and isotype control for one hour at 4°C, followed by incubation with 100 µl anti-human IgG-PE (Cat# 409304, biolegend) for one hour at 4°C. The mean fluorescence intensity (MFI) was calculated using GraphPad Prims software version 7.0 and was plotted against the protein concentration. The mAbs/cell was determined making a standard curve using beads from Quantibrite (BD biosciences).

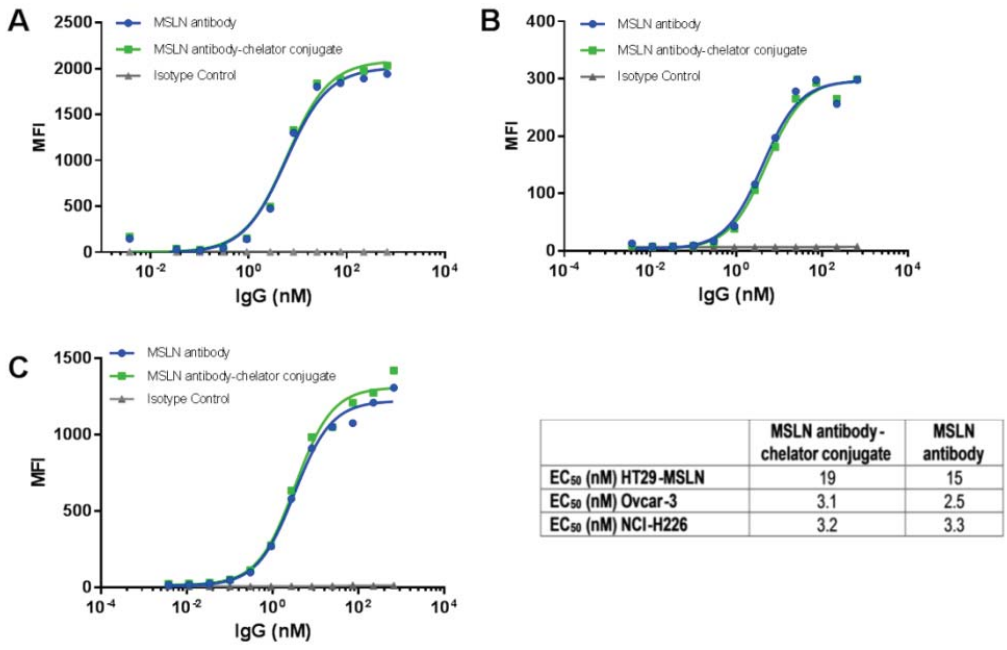

	MSLN antibody-chelator conjugate	MSLN antibody
EC_{50} (nM) HT29-MSLN	19	15
EC_{50} (nM) Ovcar-3	3.1	2.5
EC_{50} (nM) NCI-H226	3.2	3.3

Figure 1. FACS analysis on different cell lines, comparing binding potency of naked MSLN antibody with MSLN-antibody conjugate. An isotype control conjugate was included to demonstrate specificity. Data were fitted using Graph Pad Prism software, EC50 values are presented in the table. Binding to **A)** HT29-MSLN cells; **B)** Ovcar-3 cells; **C)** NCI-H226 cells

Figure 2: ELISA on recombinant human MSLN.

For ELISA, recombinant human MSLN was coated to 96-well plates (1 µg/mL; NUNC/Maxisorp). Wells were blocked with 3 % BSA in PBS. Cold MSLN-antibody conjugate, an isotype control antibody and the radiolabeled MSLN-TTC (7 MBq/10mg, stored for 72 hours) were titrated (1:3; 100 µg/mL) on the MSLN coated ELISA plate. Unbound samples were washed off and bound samples were visualized using horseradish peroxidase labeled goat anti-human lambda antibody (Southern Biotech) followed by visualization with the peroxidase substrate ABTS (Life Technologies). The absorbance was measured at 405 nm in a plate reader (Perkin Elmer). EC_{50} values were calculated using GraphPad Prism Software.

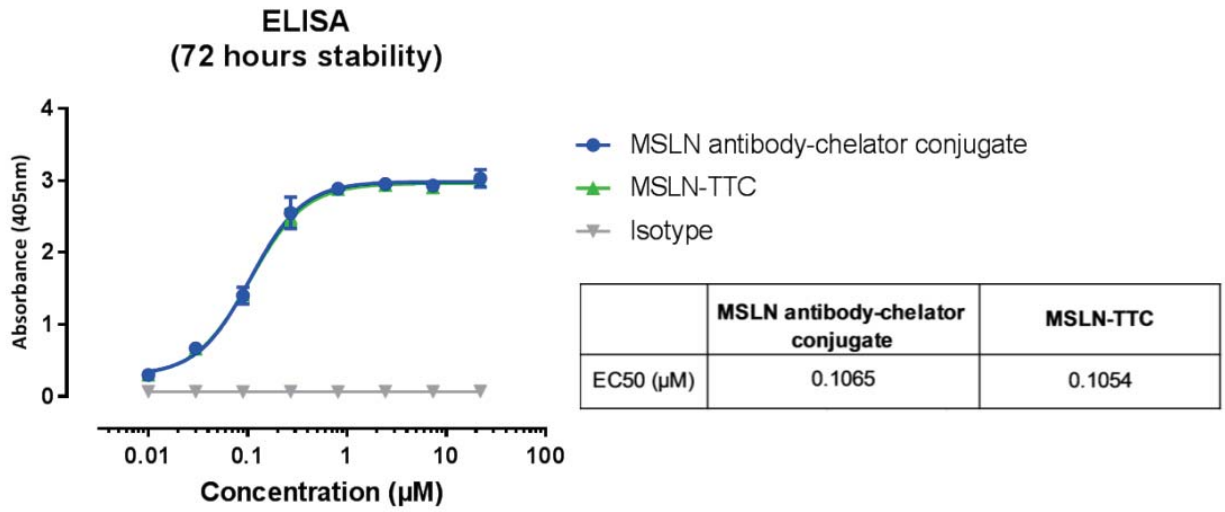

	MSLN antibody-chelator conjugate	MSLN-TTC
EC50 (µM)	0.1065	0.1054

Figure 2. ELISA on recombinant human MSLN. Binding affinity of the radiolabeled MSLN-TTC (7 MBq/ 10 mg) is compared against the antibody-chelator conjugate and isotype control after 72 hours incubation, demonstrating no change in binding affinity.

Figure 3: Isobologram Generated from CAPAN-2 Cell Line Treated with MSLN-TTC in Combination with DDR Inhibitors.

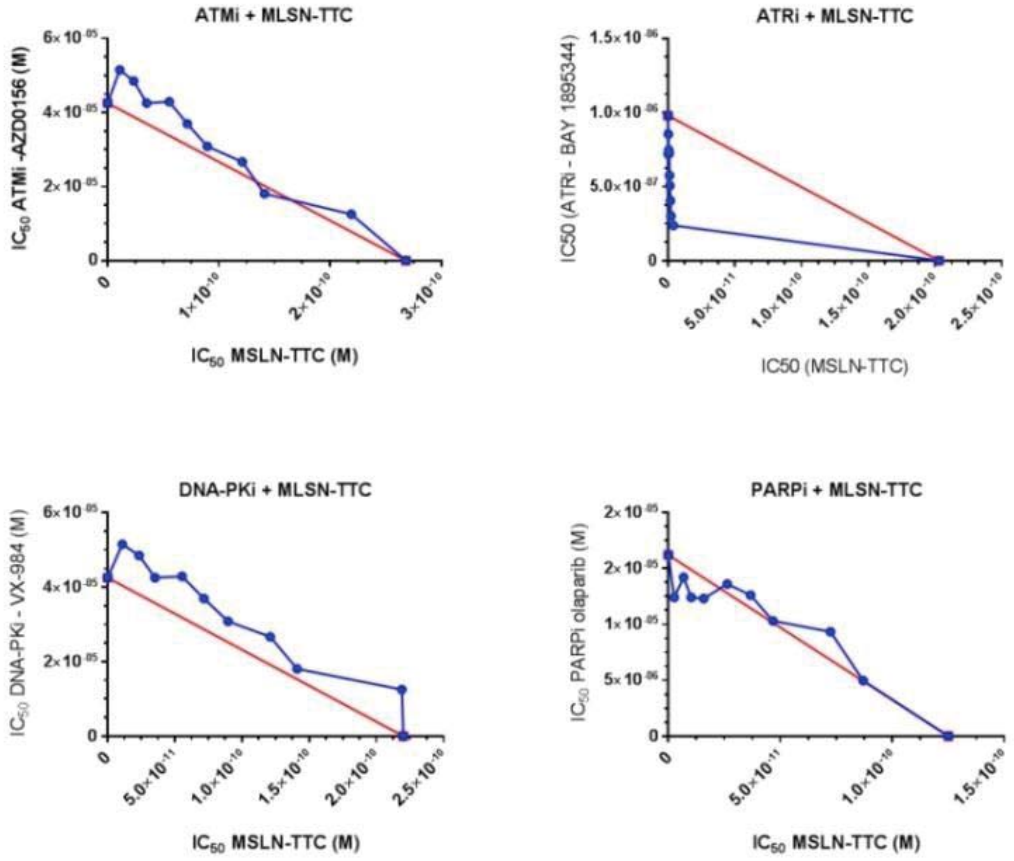

Figure 3. Isobologram generated from CAPAN-2 cell line treated with MSLN-TTC in combination with DDR inhibitors. Cell viability was determined by use of CellTiterGlo. The IC_{50}-isobolograms were generated by plotting the actual IC_{50} values of MSLN-TTC and DDRi along the x- and y-axis, respectively.

Figure 4: Isobologram generated from HT29-MSLN Cell Line Treated with MSLN-TTC in Combination with DDR Inhibitors.

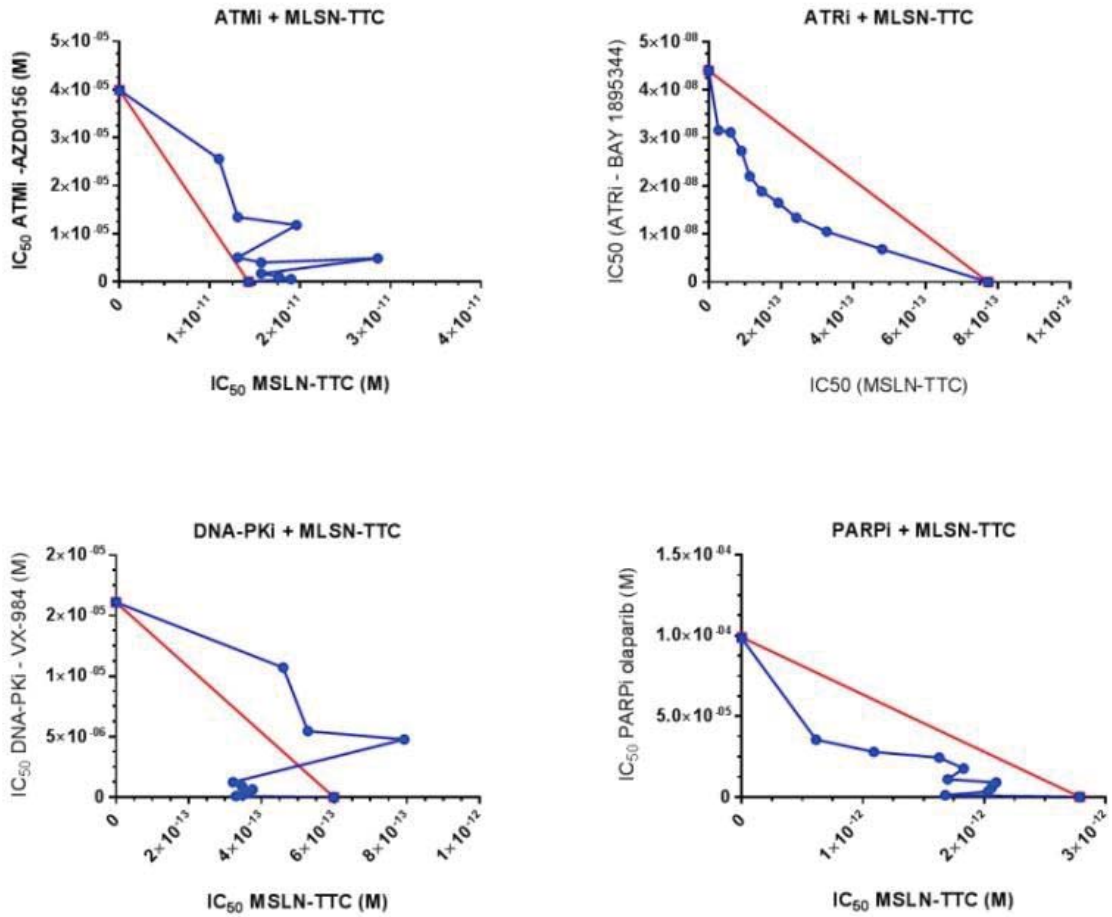

Figure 4. Isobologram generated from HT29-MSLN cell line treated with MSLN-TTC in combination with DDR inhibitors. Cell viability was determined by use of CellTiterGlo. The IC_{50}-isobolograms were generated by plotting the actual IC_{50} values of MSLN-TTC and DDRi along the x- and y-axis, respectively.

Figure 5: **Isobologram generated from NCI-H226 Cell Line Treated with MSLN-TTC in Combination with DDR Inhibitors.**

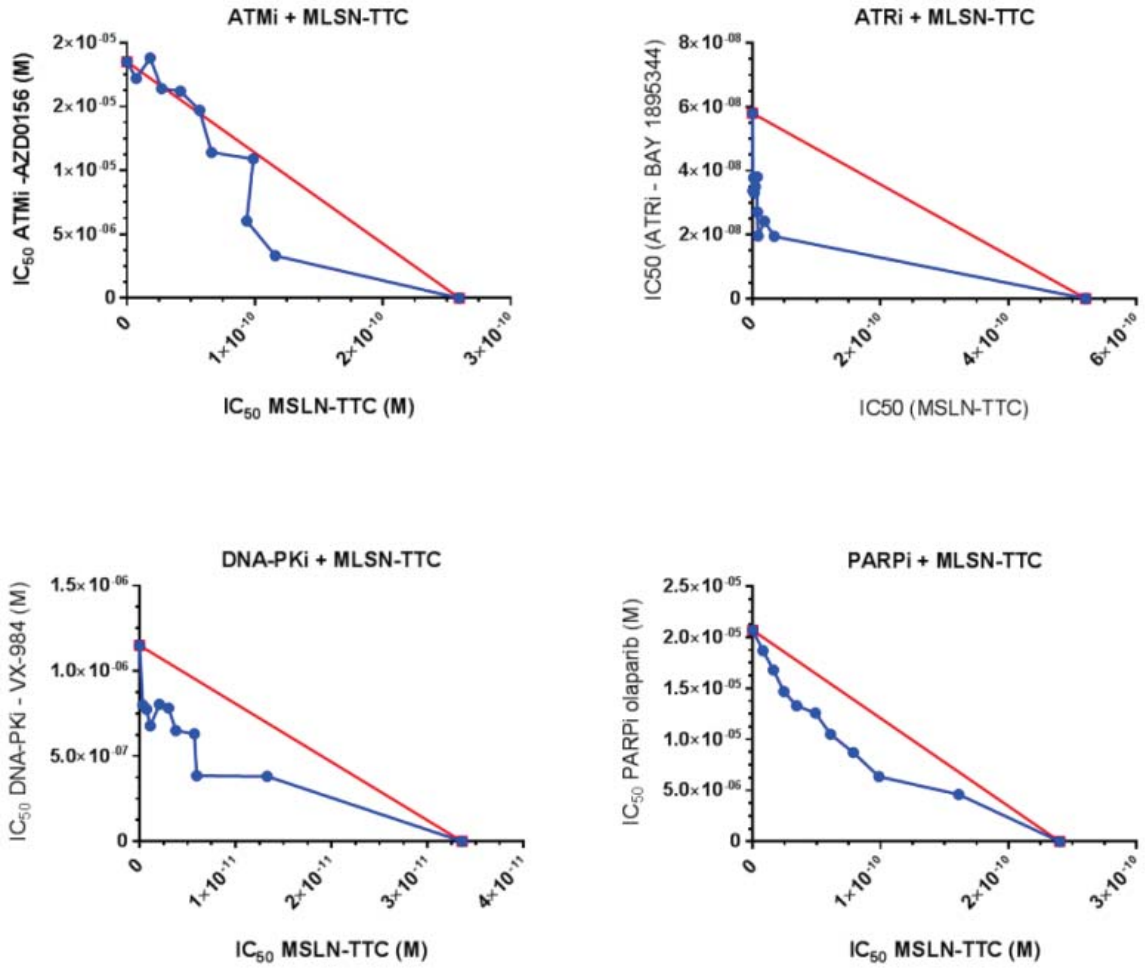

Figure 5. **Isobologram generated from NCI-H226 cell line treated with MSLN-TTC in combination with DDR inhibitors.** Cell viability was determined by use of CellTiterGlo. The IC_{50}-isobolograms were generated by plotting the actual IC_{50} values of MSLN-TTC and DDRi along the x- and y-axis, respectively.

Figure 6: Isobologram generated from OVCAR-8 Cell Line Treated with MSLN-TTC in Combination with ATR Inhibitor.

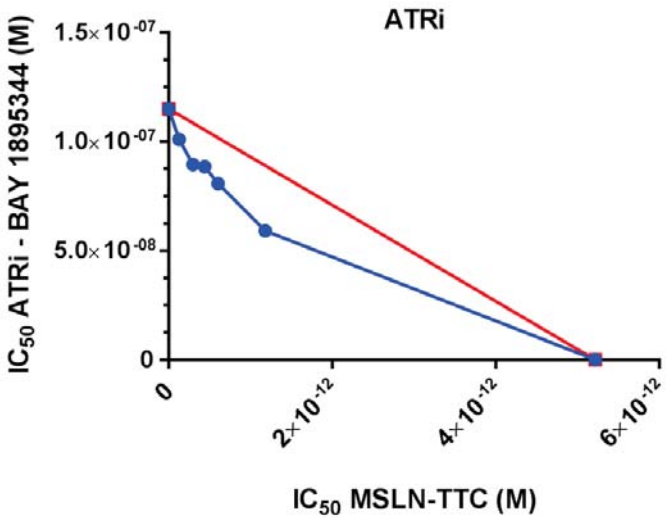

Figure 6. Isobologram OVCAR-8 treated with MSLN-TTC in combination with ATRi. Cell viability was determined by use of CellTiterGlo. The IC_{50}-isobolograms were generated by plotting the actual IC_{50} values of MSLN-TTC and DDRi along the x- and y-axis, respectively.

Figure 7. *In Vitro* Experiments from MSLN-TTC +/- ATRi BAY 1895344 or PARPi olaparib on OVCAR-3

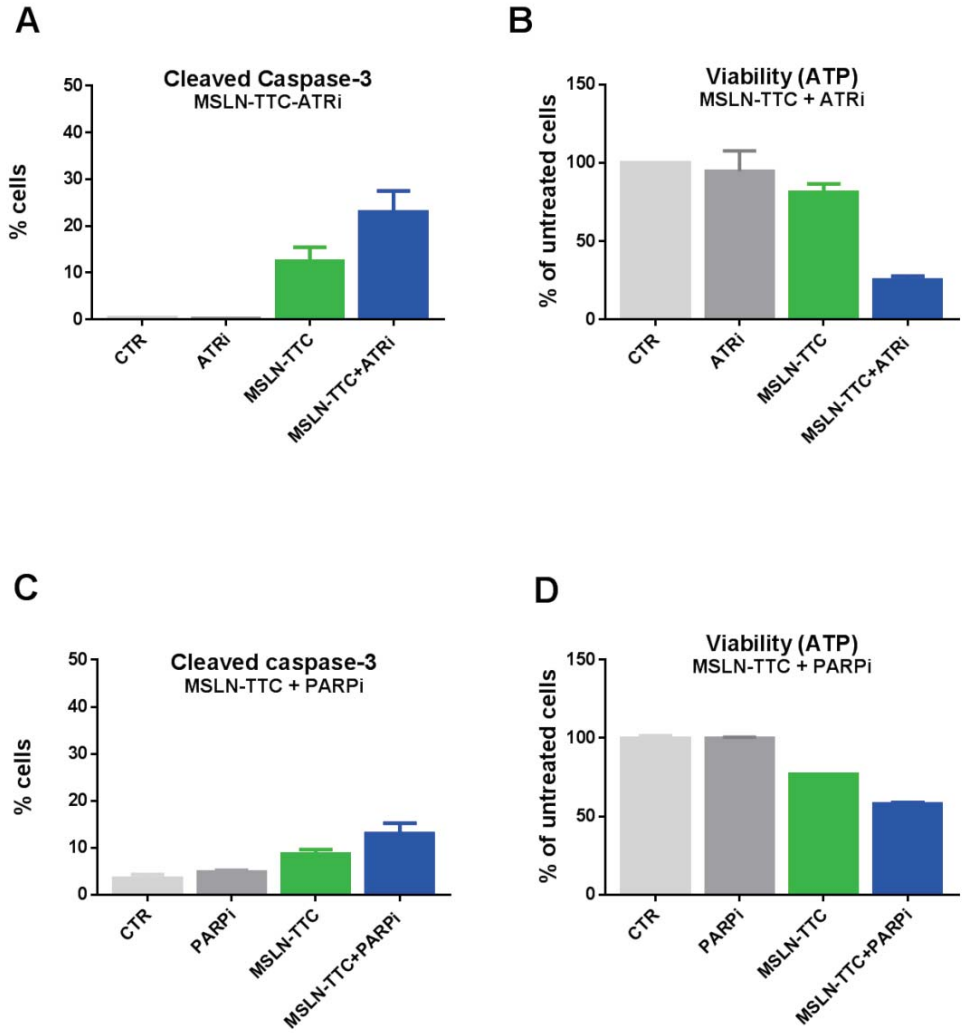

Figure 7. *In vitro* experiments from MSLN-TTC +/- ATRi BAY 1895344 or PARPi olaparib on OVCAR-3. A-B) Apoptosis and viability determination after combination treatment with MSLN-TTC (10 kBq/ml) and BAY 1895344 (10 nM). C-D) Apoptosis and viability determination after combination treatment with MSLN-TTC (1 kBq/ml) and olaparib (0.5 µM).

Supplemental table 1 and 2: Mean Values ± SD of Mechanistic Markers

Table 1: Mean Values ± SD of Mechanistic Markers MSLN-TTC + ATRi

Marker	CTR	MSLN-TTC	ATRi	MSLN-TTC + ATRi
DSB (γH2A.X)	5.3 ± 1.0	26.3 ± 2.1	6.3 ± 0.5	43.3 ± 1.8
Apoptosis (Cleaved Caspase-3)	0.4 ± 0.3	12.45 ± 3.0	0.3 ± 0.3	23.0 ± 4.5
Viability (ATP)	100 ± 0.5	81.1 ± 5.5	94.5 ± 2.4	25.3 ± 2.4

Table 2: Mean Values ± SD of Mechanistic Markers MSLN-TTC + olaparib

Marker	CTR	MSLN-TTC	olaparib	MSLN-TTC + olaparib
DSB (γH2A.X)	4.6 ± 1.2	29.6 ± 0.7	10.8 ± 0.4	35.8 ± 3.5
Apoptosis (Cleaved Caspase-3)	3.5 ± 0.8	8.7 ± 1.0	4.9 ± 0.4	13.1 ± 2.1
Viability (ATP)	100 ± 1.5	76.9 ± 0.2	99.8 ± 0.8	57.8 ± 1.3

Figure 8: Body Weights Determined after Treatment with MSLN-TTC in Combination with ATRi BAY 1895344 or PARPi olaparib.

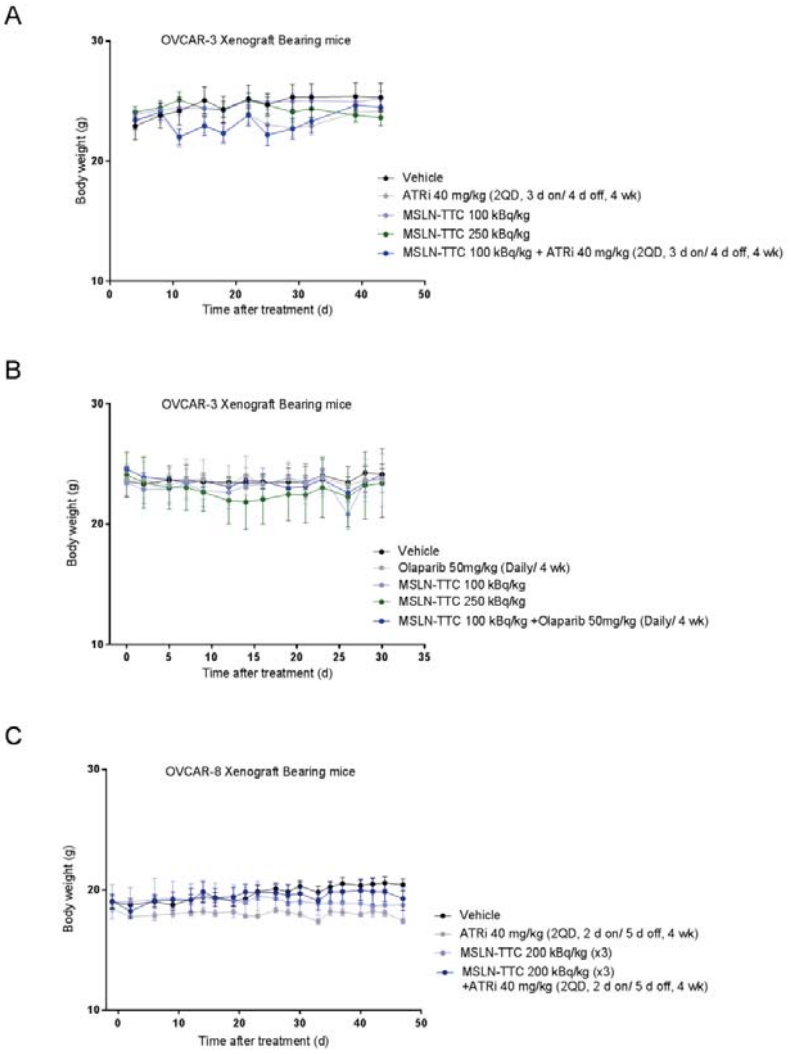

Figure 8. Body weights determined after treatment with MSLN-TTC in combination with ATRi BAY 1895344 or PARPi olaparib. A) Body weight of OVCAR-3 xenograft bearing mice determined after a single dose administration of MSLN-TTC (100 kBq/kg, 0.14 mg/kg, i.v.) and ATRi (40 mg/kg 2QD, 3 days on/ 4 days off, 4 weeks), B) Body weight of OVCAR-3 xenograft bearing mice determined after a single dose administration of MSLN-TTC (100 kBq/kg, 0.14 mg/kg, i.v.) and olaparib (50 mg/kg QD for 4 weeks), C) Body weight of OVCAR-8 xenograft bearing mice determined after three intravenous (i.v.) injections of MSLN-TTC (200 kBq/kg, 0.14 mg/kg, day 1, 22 and 43) and BAY 1895344 (40 mg/kg 2QD, 2 days/5 days off, 7 weeks).